UNIVERSIDADE FEDERAL DE SÃO CARLOS
CENTRO DE CIÊNCIAS EXATAS E DE TECNOLOGIA
DEPARTAMENTO DE QUÍMICA
PROGRAMA DE PÓS-GRADUAÇÃO EM QUÍMICA

Gels and Sponges Nanocomposites based in Chitosan, Poly (N-Vinyl Caprolactam) and SiO_2 applied as Drug Delivery System

Fiama Martins Cutrim*

Tese apresentada como parte dos requisitos para obtenção do título de DOUTORA EM CIÊNCIAS, área de concentração: FÍSICO-QUÍMICA

Advisor: Emerson Rodrigues de Camargo

Coadvisor: José das Neves (Universidade do Porto-Portugal)

*** Fundação de Amparo à Pesquisa do Maranhão**

São Carlos - SP

2023

UNIVERSIDADE FEDERAL DE SÃO CARLOS

Centro de Ciências Exatas e de Tecnologia

Programa de Pós-Graduação em Química

Folha de Aprovação

Defesa de Tese de Doutorado da Candidata Fiama Martins Cutrim, realizada em 14/06/2023

Comissão Julgadora:

Prof. Dr. Emerson Rodrigues de Camargo (Orientador)

Profa. Dra. Simone Milani Brandão (DeMed/UFSCar)

Profa. Dra. Dayane Batista Tada (UNIFESP-São José dos Campos)

Profa. Dra. Tatiana Santana Ribeiro (UFSCar-Araras)

Prof. Dr. Caio Sampaio (FOA/Unesp)

O presente trabalho foi realizado com apoio da Fundação de Amparo à Pesquisa do Maranhão (FAPEMA) – Solicitação BD-02176/19.

O relatório de Defesa assinado pelos membros da Comissão Julgadora encontra-se arquivado junto ao Programa de Pós-Graduação em Química

Meu único defeito é não ter medo de fazer o que gosto

Dedication

I dedicate this thesis to my family and friends. I dedicate it to my parents, Adalberto José Cutrim and Raimunda Iraneide Martins Cutrim, for the life, love, and education they gave me. My sister Elizia da Conceição Martins Cutrim was also like a mom for many years and encouraged me to be the better I am.

My husband, Moisés Rocha dos Santos, is also my best friend and has been with me during my academic journey and motivated me to continue despite the difficulties we face.

ACKNOWLEDGEMENTS

I thank the committee for the precious time and knowledge dedicated to reading and improving this work.

I thank my advisor Emerson Rodrigues de Camargo, for his time, dedication, knowledge, and kindness. During these years, he teaches and guides to do a good job and be patient during the pandemic.

I want to acknowledge to Nanomedicines and Translational Drug Release Group. Thank you, Professor Bruno Sarmento and Dr. José das Neves, for receiving me at the Institute for Research and Innovation in Health, where I could perform part of this work and had the best year of my Ph.D. You teach me a lot and motivate me to overcome my limitations.

Thank you, Professor Thiago Venâncio from the NMR laboratory from UFSCar, for helping us to elucidate the chemical characterization of the materials presented in this work.

Thank you, Dr. Daniella Lure Morgado, for being part of this work with me, for the great contribution, your experience, friendship, and kindness.

Thank you, Arthur Martins Gabriel, for contributing to the differential scanning calorimetry, and Guilherme Arioli for his precious help in the experimental work in the last months in Brazil before my internship in Portugal.

Thank you, Dr. Josiane Carneiro Souza, for your precious contribution to the thermogravimetric analysis and your friendship.

Thank you, Beatriz Rocha and Sofia Barros, for the cell culture training and your kindness and friendship.

Thank you, Lisa Salguero, for your help in my biomechanical assays, for sharing your experience, and for suitable suggestions.

Thank you, Juliana Veigas, for sharing your experience in pharmaceutical sciences, always being available to help me and all the colleagues, and for your friendship.

Thank you to all my friends from UFSCar and I3s, especially: Daniela Morgado, Regiane Oliveira, Wyllamanney Silva Sczancoski, Aline Barros, Francisco Nunes de Souza Neto, Luís Fernando Gorup, Gleison Neres Marques, Paulo Faria, Cristina Santarcangelo, Miriam Campolo, Larissa Spósito, Natália Costa, Melike Sessevmez, Amir Soleimany, Soraia Pinto, Krisztián Pamlényi, Helena Almeida, Barbara Ferreira, Margarida Carvalho, Diogo Coelho, Diogo Horta, Sofia Dias, Sofia Barros, Sofia Costa,

Catarina Pacheco, Sonia Siquenique, Wedja Vieira, Seem Awad and Juliana Veigas. I enjoy every single moment with you.

I am enormously grateful to Fundação de Amparo à Pesquisa do Maranhão for the financial support it gives by the process EDITAL Nº 005/2019 DOUTORADO NO PAÍS, to the grant #2013/07296-2, São Paulo Research Foundation (FAPESP) and to Coordenação de Aperfeiçoamento de Pessoal de Nível Superior - Brasil (CAPES) - Finance Code 001.

Thank the Department of Chemistry of Federal University of São Carlos and the Center for the Development of Functional Materials – CDFM for all the research structure and financial support.

Thanks to the Ybitec P&D em Nanotecnologia where I can perform part of my experiments.

I want to acknowledge to Institute for Research and Innovation in Health from Porto University for the research structure and financial support.

FIGURES LIST

TABLE LIST

ABBREVIATION LIST

LCST – Lower Critical Solution Temperature
CTZ – Clotrimazole
Ch – Chitosan
PNVCL – Poly (N-Vinyl Caprolactam)
DDS – Drug Delivery System
VVC – Vulvovaginal Candidiasis
MIC - Minimum Inhibition Concentration
MFC - Minimum Fungicide Concentration

RESUMO

GÉIS E ESPONJAS NANOCOMPÓSITOS A BASE DE QUITOSANA, POLI (N-VINIL CAPROLACTAMA) E SIO_2 APLICADOS COMO SISTEMAS DE LIBERAÇÃO DE MEDICAMENTOS. Quitosana é um biomaterial promissor para ablicação biológica como em sistemas de liberação de medicamentos (DDS) devido a características como biocompatibilidade, responsividade catiónica, ajuste da morfologia, podendo formar nanopartículas, filmes, esponjas, etc. Por isso, esse estudo reporta os resultados da síntese e caracterização de compósitos de quitosana com poli (n-vinil caprolactama) (PNVCL) e SiO_2 para aplicação como DDS para o tratamento de candidíase vulvovaginal (VVC). Foram obtidas esponjas desses materiais e também esponjas carregadas com clotrimazol (CTZ). As propriedades físico-químicas estudadas, mostraram que os materiais possuem características térmicas adequadas considerando sua aplicação. O estudo das propriedades biomecanicas mostraram que os compósitos são adequados para aplicação e que a rigidez pode ser ajustada com a inserção de PNVCL ou PNVCL-SiO_2. Os materiais foram testados para atividade anti *candida* na qual observou-se que a atividade do fármaco foi mantida com sua associação aos biomateriais. O estudo da citotoxicidade usando linhas celulares do trato vaginal feminino indicou a biocompatibilidade dos materiais. De acordo com os resultados, as esponjas de quitosana e seus compósitos são promissoras para aplicação no tratamento de candidíase vulvovaginal devido à sua capacidade de manter a atividade do fármaco e serem biocompatíveis.

ABSTRACT

GELS AND SPONGES NANOCOMPOSITES BASED IN CHITOSAN, POLY (N-VINYL CAPROLACTAM) AND SIO_2 APPLIED AS DRUG DELIVERY SYSTEM. Chitosan (Ch) is a suitable biomaterial for biological applications like drug delivery systems (DDS) due to biocompatibility, cationic responsiveness, and adjustable morphology forming nanoparticles, films, sponges, etc. For these reasons, this study reports the results of the synthesis and characterization of chitosan composite with poly (n-vinyl caprolactam) (PNVCL) and SiO_2 for the application as DDS for the treatment of vulvovaginal candidiasis (VVC). The materials loaded with clotrimazole (CTZ) were obtained. The physical-chemical properties show that the materials have good thermal stability considering the application. The biomechanical properties are adequate and can be adjusted according to the insertion of PNVCL or PNVCL-SiO_2. The materials were tested for activity against *Candida* species, and the antifungal activity was maintained with the drug associated with the materials. Cytotoxicity studies using female genital tract cell lines were performed, showing biocompatibility. According to the results obtained so far, the chitosan sponges and its composites appear to be an excellent formulation to be used in the treatment of VVC because they can maintain the antifungal activity of CTZ and due to their biocompatibility.

SUMÁRIO

1 - INTRODUCTION

Currently, there is a large quantity of biomaterial that can be applied to the health sciences, like biosensors, implants, tissue bio-regeneration supports, and the release of medicines (BRONZE-UHLE *et al.*, 2019; CULVER; CLEGG; PEPPAS, 2017; FERREIRA *et al.*, 2019; GOESMANN; FELDMANN, 2010; PARVEEN; MISRA; SAHOO, 2012). The drug delivery systems may be revised for every newly discovered medicine to ensure the appropriate release rate. This study is essential to avoid intoxication or inefficiency and ensure the molecule's protection in physiological conditions (CULVER; CLEGG; PEPPAS, 2017).

Many biocompatible nanoparticles are applied to protect from chemical attacks or to control the release rate (TANG; LI; CHEN, 2012; WANG *et al.*, 2015). The insertion of nanoparticles in polymeric matrices allows the combination of material properties to increase the shelf life. Hybrid biomaterials can cross biologic barriers, respond the external stimulus as pH and temperature, have good biocompatibility in vitro and in vivo, and some of them can present antimicrobial activity (ALI; AHMED, 2018; MOHAMMED; BIN YUSOH; SHARIFFUDDIN, 2018).

Polymeric materials, especially hydrogels, can present tridimensional networks that can absorb high quantities of water or physiologic solution suitable for drug delivery systems (ALI; AHMED, 2018). Several administration routes are dependent on the acting region of the drug. Although oral delivery is the most common for several diseases due to the simplicity and to be pain-free, the drug must cross the intestinal tract before reaching the affected region. The consequence is a reduction of the bioavailability of the drug, and several dosage administrations may be necessary to obtain the therapeutic effect. However, there are additional administration routes that consider the application directly in the affected organ, without passing through the intestinal tract, for example., the intravenous that has the advantage of high bioavailability *in vivo* and the via topic in which the vehicle must cross the skin for the molecule action.

Many biomaterials can promote stimulus responsiveness in the physiological medium. Chitosan (Ch), for example, is a natural biocompatible polymer with cationic properties capable of responding to pH variation and absorbing a large quantity of aqueous media, being an interesting material to be used as a drug delivery system (DDS). Chitosan can be used in many forms like hydrogel, film, nanoparticles,

and sponges (FACCHINATTO *et al.*, 2021; HAN *et al.*, 2014a; MONTEMBAULT; VITON; DOMARD, 2005; REZAEI *et al.*, 2021). Another stimulus-responsive biomaterial is the poly (N-vinyl caprolactam) (PNVCL), a polymer obtained from the radical polymerization of N-vinyl caprolactam that is thermosensitive. This material presents a sol-gel transition near the physiological temperature. Above a value called lower critical solution temperature (LCST), the interaction between the polymer chain is stronger than the polymer with water(RL *et al.*, 2017). The polymer changes its conformation from a coil to a globule above the LCST. One of its practical applications is that in the globule conformation, PNVCL can encapsulate molecules in its structure. The transition change can be used as a mechanism for drug delivery stimulated by temperature change (MOHAMMED; BIN YUSOH; SHARIFFUDDIN, 2018; RL *et al.*, 2017).

Considering the different medical applications of biomaterials in the vulvovaginal route, materials like poly(pseudo)rotaxanes, polymers based on amphiphilic molecules, and cyclodextrins were studied as DDS for candidiasis in the form of gel(COSTA *et al.*, 2023). Cautela and coworkers studied a composite biomaterial based on polyvinyl alcohol and pectin as a vaginal film containing microbicides to prevent the sexual transmission of HIV (CAUTELA *et al.*, 2019). Vaginal sponges also gain space with biomaterials like chitosan applied as DDS for sildenafil citrate to enhance uterine blood flow (Aboudet al., 2018). The enhancement of its blood flow increases the vasodilatation of endometrial vasculature, favoring *vitro* pregnancy(ABOUD *et al.*, 2018).

The vulvovaginal tract can be naturally susceptible to diseases (Das Neves et al., 2008). Many fungus species exist in the human mucosal microbiome (KHOSRAVI *et al.*, 2018). The *Candida* spp. is an opportunistic pathogeny that causes candidiasis in susceptible individuals with clinical manifestations, like subcutaneous ulcers, itching, hyperkeratosis of skin, deformation, and edema of the fingernails, depending on the species(KHOSRAVI *et al.*, 2018; ROJZ *et al.*, 2022; WU, JUAN *et al.*, 2021). Vulvovaginal candidiasis is an infection that affects 75% of women at least once in their lifetime, commonly associated with long-term antibiotics and sexual transmission(DENNING *et al.*, 2018).

This thesis presents the applying sponge’s hybrid biomaterials based on chitosan, PNVCL, and SiO_2 as DDS. For this purpose, these materials' synthesis and physical-chemical were fully explored to determine their properties for use as a DDS

in the vaginal mucosa. The sponges were loaded with clotrimazole, an antifungal molecule from the azoles group. The materials were studied according to the anti-*candida* activity, cytotoxicity in epithelial cell lines of the female genital tract, permeability, and drug release.

2 - LITERATURE

2.1 - Pharmacokinetics and Drug Release

Pharmacokinetics comprehends the physiological answer of the organism with the presence of a drug (ROBERTS; TACCONE; LIPMAN, 2015). When a prescription is administrated to the body, four pharmacokinetics mechanisms can occur: absorption, distribution, biotransformation or metabolism, and elimination (CAVALHEIRO; COMARELLA, [S.d.]).

The absorption step describes the enter and assimilation of the drug through the blood circulation until the target cell. The absorption process can occur by active diffusion, in which there is energetic consumption, and passive, in which there is no energy consumption. The transportation can occur by paracellular diffusion, lipidic, transcytosis, and nanocarrier molecules(G. KATZNUNG, 2014; REINHOLZ; LANDFESTER; MAILÄNDER, 2018)**.**

In paracellular transport or aqueous diffusion, the molecules pass through the spaces of the epithelial membrane, which are very compacted barriers that usually only small species can cross. In lipidic distribution, the drug can be dissolved in the lipidic layer, which presents a lot of obstacles with aqueous compartments. So, a factor that determines this kind of absorption is the lipidic-aqueous partition coefficient of the drug (G. KATZNUNG, 2014; REINHOLZ; LANDFESTER; MAILÄNDER, 2018). Transcytosis is a mechanism in which a macromolecule is linked to a receptor in the cell surface, forming a vesicle that can transport the drug to the intracellular environment – endocytosis-or the reverse process- exocytosis. The nanocarriers are molecules in the cell and insoluble in the lipidic medium. These molecules can transport species to the intern or extern of the cells (G. KATZNUNG, 2014; REINHOLZ; LANDFESTER; MAILÄNDER, 2018).

The distribution step consists in the quantity of drug that reaches the intracellular region or around the cell(HOLFORD, 2014). The drug can reach the blood system in the free form or linked to the plasm protein. When the drug comes to the target cell, its free state in the blood is in equilibrium with the intra and extracellular environment. As the concentration of free-form drugs decreases, the linked one will be detached from the plasm protein and available to act in the tissues. The drug

concentration can vary according to the interactions with organs or tissues in study, physical chemical properties, age, and patient weight (Holford, 2014).

The biotransformation consists of a drug metabolization process, possible in specie with lesser pharmacological properties than the original molecule or in an inactive one that can be easily eliminated. The elimination of small molecules soluble in physiological pH can occur via renal (CORREIA, 2014). However, many drugs can be liposoluble and have a long time linked to the plasm protein. In these cases, other metabolism routes can occur, like oxidation and hydrolysis of the molecule (CORREIA, 2014).

The elimination step occurs mainly via the renal or liver, but other organs can do it, like the lung. An important factor about this process is that when the drug concentration is high, the elimination can be harmed because the molecule will saturate these organs and will be retained for a long time, which is typical behavior in many administration routes. For this reason, one of the motivations for developing controlled drug delivery systems is to avoid administering high drug concentrations (HOLFORD, 2014).

There are a lot of drug administration routes, like oral, nasal, pulmonary, transdermal, and intravenous. However, not all can pass to the absorption step, and some can be directly administrated to the target region (LIN *et al.*, 2018). The via oral is the most common administration route for drug delivery. There are many reasons, like easiness, non-invasive administration, and free pain. However, this administration route presents limitations, like the necessity of several dosages to guarantee bioavailability because part of the initial concentration is lost during gastrointestinal transport (REINHOLZ; LANDFESTER; MAILÄNDER, 2018).

Several drug delivery systems (DDS) have been developed to encapsulate and deliver drug in target cells. Some of the most popular biomaterials used for this purpose are polymer, ceramic, and composites that also can pass to the mechanisms of absorption, distribution, biotransformation, and elimination (G. KATZNUNG, 2014; LIN *et al.*, 2018; REINHOLZ; LANDFESTER; MAILÄNDER, 2018). Intelligent biomaterials like polyacrylic acid and chitosan can encapsulate drugs andromote changes in the liberation profile due to cationic responsiveness (LIN *et al.*, 2018). Chitosan is also a mucoadhesive polymer, which can be applied to favor the absorption process in DDS in a topical application (LIN et al., 2018). Poly-(N-Vinylcapralactam) – PNVCL is another biopolymer with responsive behavior suitable

for DDS. This thermoresponsive polymer presents a sol-gel transition in temperature near the physiological medium (CORTEZ-LEMUS; LICEA-CLAVERIE, 2016).

The use of intelligent biomaterials in DDS can be able to adjust pharmacokinetics parameters, like the process of absorption and distribution. The strategic use of biomaterials properties can produce DDS to cross physiological barriers, enhance bioavailability and deliver the drug to the target tissues(HOLFORD, 2014; LIN *et al.*, 2018; REINHOLZ; LANDFESTER; MAILÄNDER, 2018).

2.1.1 Mathematical Models of drug release

The drug release is studied by the pharmacokinetics parameters to determine the velocity of absorption, distribution, metabolism and elimination of the drug. This study can be more deeply explored by the understanding of the mechanism of the drug dissolution in the physiological medium. There are many mechanisms that can happen in the drug liberation from a matrix, for example the erosion, the diffusion and, the swelling.

Normally, the mechanism of dissolution governs the velocity of the drug release. For example, the material processing and its physical chemical properties can lead to rapid increase of drug concentrations during the initial time that is commonly known as burst release (COSTA; MANUEL; LOBÔ´´, 2001; HUANG; BRAZEL, 2001) .

The dissolution velocity, the presence of burst release and the release mechanism are some information that can be obtained by the mathematical models like zero order, first order, Higuchi, Hixson-Crowell, Korsmeyer-Peppas and Weibull. In this chapter these equations will be explained in more details.

Zero Order

The zero order kinetic models describe mechanisms in which the drug solubility rate is constant over the time. The drug solubility is not affected by its concentration and its constant rate is dependent only on the time. The release of a non-disaggregated dosages is very slow over the time is described by the equation 1.

$$W_0 - W_i = K.t \qquad (1)$$

Where W_0 is the initial concentration, W_i is the remaining concentration at a t time and K is the rate constant. Dividing this equation by W0, we obtain the equation 2.

$$f_i = K_0 t \qquad (2)$$

Where f_i = 1-(Wi/W0) represents the fraction of the remaining drug at t time. The graph of f_i vs time is a straight line if the correlation coefficient was good. This model are interesting from the therapeutical perspective to avoid the fast absorption and elimination process, that leads to the necessity of frequent dosages over the time.

First Order

The first order kinetics describes a dissolution process in which the concentration is time dependent. The release is proportional to the drug concentration remaining in the interior of the DDS. So that, the drug release rate tends to diminish over the time. The equation 3 describes the first order release.

$$LogQ = LogQ_0 + \frac{K_1}{2.303} \qquad (3)$$

Where Q is the amount of the drug at t time, Q_0 is the initial amount and K_1 is the first-order constant. The graph of log Q vs time is a straight line.

Higuchi Model

Higuchi describes for the first time a model for molecules release from a solid or semisolid matrix submitted to a diffusion medium. The models consider the dissolution and the diffusion that are mechanism commonly observed in controlled drug release. Higuchi proposed an equation that predict the release of a drug in a matrix concentration lower than its solubility, in which the molecule is absorbed through the porous of the DDS (equation 4).

$$f_1 = Q = \sqrt{\frac{D\varepsilon}{\tau}(2C - \varepsilon C_{(S)})C_S T} \qquad (4)$$

Where f1 and Q is the quantity of drug released at a t time by area unit, Ɛ is the matrix porosity, τ is the capillary tortuosity factor, C is the initial amount of drug, C_s is the solubility of the molecule in the matrix and D is the diffusion coefficient of the matrix.

Hixson-Crowell

This mathematical model is applicable to those DDS, like tablets, in which the dissolution occurs over plans in the surface area. The area and the volume tend to decrease over the dissolution time, but the form is maintained. Hixson and Crowell describes the dissolution process and the area of a DDS is proportional to the cubic root of its volume according to the equation 5.

$$\sqrt[3]{W_0} = \sqrt[3]{W_i} + K_{HC} \qquad (5)$$

Or simplifying, the equation 6 is obtained

$$\sqrt[3]{1 - f_i} = 1 - K_{HC} \qquad (6)$$

f_i = 1-(Wi/W0) represents the fraction of the remaining drug at t time and K_{HC} is the release constant.

Korsmeyer-Peppas

This model describes a drug release from a polymeric matrix and is known as power law. It is normally used when the release mechanism is not well known or more than one is involved. Using this model is possible to define if the mechanism occurs by diffusion, polymer relaxation or both. Using the equation 7 describes a linear curve of logarithm of cumulative release versus logarithm of the time.

$$LogQ = LogK_{RP} + nLog\,(t - l) \qquad (7)$$

Where Q is the cumulative drug release over the t time, K_{RP} is the kinetic constant, l is the is the latency time, and n is the exponent of release, that characterizes the mechanism that occurs. When n=0.5 the mechanism is diffusion (Fickian model case I). The diffusion rate is higher than the process of polymer relaxation. When n=1, the non-Fickian drug release is governed by the swelling or relaxation of polymeric chains. When 0.5<n<1 a non-Fickian anomalous case characterizes a mechanism governed by diffusion and swelling. And when n>1, another non-Fickian model describes a case where the sorption, tension and breaking of polymer occurs.

When an abrupt release occurs in the initial time (burst effect) the following equation 8

$$Q = Kt^n + b \quad (8)$$

Where b is the burst effect. As higher as b value, higher is the concentration over a short period of time (HUANG; BRAZEL, 2001; KIM; FASSIHI, 1997) .

Weibull

This model is indicated to describe a drug release from a matrix. The equation 9 is expressed by the cumulative drug fraction (m)

$$m = 1 - e^{-(t-Ti)^{\frac{b}{a}}} \quad (9)$$

Where a describes the timescales of the process, Ti is the latency time and b is the type of the curve that has also a correlation with n Fickian diffusion. The natural logarithm of negative natural logarithm of m versus the natural logarithm of the time have a linear fitting with several drug release profile and the slope of this curve provide the b value that give information about the type of curve. When b=1 the curve shape is an exponential, b>1 is a sigmoidal and b<1 describes a parabolic graph.

2.2 Vulvovaginal Candidiasis

Candidiasis, also known as a yeast infection, is a common fungal infection caused by the overgrowth of Candida species, particularly Candida albicans. Candida is a type of yeast that normally resides in the human body, including the skin, mouth, digestive tract, and genital area, without causing any harm. However, certain factors can disrupt the balance of microorganisms in the body, leading to an overgrowth of Candida and the subsequent development of candidiasis (DENNING *et al.*, 2018; WU *et al.*, 2021).

There are various types of candidiasis, each affecting different parts of the body. Vaginal yeast infections are prevalent type, characterized by itching, burning, and a thick, white discharge. Vulvovaginal candidiasis, commonly known as a yeast infection, is a type of fungal infection that affects the vulva and vagina in women. It is primarily caused by the overgrowth of Candida species, particularly *Candida albicans*. But *C. glabrata* and *C. Krusei* are non *albicans* that can be also present is a candida infection (INTRA *et al.*, 2022). Candida is a type of yeast that naturally resides in the vaginal area in small amounts without causing any harm. However, certain factors can disrupt the delicate balance of microorganisms in the vaginal environment, leading to an overgrowth of Candida and the subsequent development of vulvovaginal candidiasis (FACCHINATTO *et al.*, 2021).

Several factors can contribute to the development of vulvovaginal candidiasis. These include weakened immune systems, sexual intercourse, poor personal hygiene, hormonal changes, such as those that occur during pregnancy or the menstrual cycle, as well as the use of certain medications, particularly broad-spectrum antibiotics (DOS *et al.*, 2023).

The symptoms of vulvovaginal candidiasis can vary from person to person but commonly include itching and irritation in the genitalia, redness and swelling of the vulva, a thick, white, cottage cheese-like discharge, burning sensation during urination or intercourse and soreness and discomfort in the vaginal area (INTRA *et al.*, 2022).

The diagnosis of vulvovaginal candidiasis usually involves a combination of medical history, physical examination, and laboratory tests. The healthcare professional may perform a pelvic examination to evaluate the vaginal area and collect a sample of the discharge for further analysis. This sample is typically examined under a microscope or sent to a laboratory for culture, which helps confirm the presence of Candida and rule out other possible infections (DOS *et al.*, 2023; INTRA *et al.*, 2022).

Treatment for vulvovaginal candidiasis usually involves antifungal medications. These medications are available in various forms, including creams, suppositories, and oral tablets. Over-the-counter antifungal creams or suppositories, containing ingredients such as clotrimazole or miconazole, are often effective in treating mild cases of vulvovaginal candidiasis (DOS *et al.*, 2023) .

2.2.1 Clotrimazole

Clotrimazole is an antifungal medication widely used for the treatment of various fungal infections. It is effective against a range of fungal organisms, including Candida species and dermatophytes. Clotrimazole is available in different formulations, including creams, lotions, powders, and oral lozenges (FACCHINATTO *et al.*, 2021).

Clotrimazole works by disrupting the synthesis of ergosterol, a vital component of fungal cell membranes. This disruption leads to the leakage of cellular contents and ultimately the death of the fungal organism (PAIS et al., 2016). One of the most common applications of clotrimazole is in the treatment of vaginal yeast infections, which are caused by an overgrowth of Candida species. Clotrimazole vaginal cream or suppositories are inserted into the vagina to alleviate symptoms such as itching, burning, and abnormal discharge. It helps to restore the natural balance of microorganisms in the vaginal area and relieve the discomfort associated with the infection (FACCHINATTO *et al.*, 2021).

Clotrimazole is generally presents low risk of significant side effects. In rare cases, allergic reactions may occur, characterized by swelling, itching, or difficulty breathing (ALMANGOUR et al., 2021). Depending on the specific formulation, clotrimazole may need to be applied once or twice daily for a prescribed duration. It is important to complete the full course of treatment even if symptoms improve, as discontinuing prematurely may allow the infection to return. This is a pharmacokinetic behavior called as post antifungal effect (PAFE) that is described the effect of the drug over the time in which the drug concentration is above the MIC. There are some drugs in which the regrowth is very slow, but there are others that have a rapid PAFE and in this case a continuous treatment is needed.

2.3 - Polymeric Biomaterials

Biomaterials are natural or synthetic substances that can interact with biological mediums (TIBBITT; LANGER, 2017). Polymeric materials, especially hydrogels, and sponges, can present tridimensional polymeric networks that can absorb high quantities of water or physiological fluids, with allows their use as DDS (ALI; AHMED, 2018). Many DDSs are designed for oral via the most common drug administration for many reasons, such as self-administration and free pain. Although some medicines can present low solubility in some physiological mediums, they can be degraded before they reach the target region or require the ingestion of high dosage to improve their bioavailability, which can generate problems like toxicity (CULVER; CLEGG; PEPPAS, 2017). The biomaterials can be presented in different forms, like nanoparticles, creams, solutions, hydrogels, and sponges (ABOUD *et al.*, 2018; NOROUZI; NAZARI; MILLER, 2016; TANG; LI; CHEN, 2012).

Hydrogels are biomaterials capable of retaining much water inside their 3D structure. A hydrogel can be formed with or without reticulation (CULVER; CLEGG; PEPPAS, 2017). Some can be created with external stimuli like thermo-responsive hydrogels such as PNIPAM and PNVCL that present a sol-gel transition(CORTEZ-LEMUS; LICEA-CLAVERIE, 2016).

Sponges are high porous materials that can absorb a large quantity of water. These materials can be formed based on sol-gel transition, gas injection, freeze-drying, electrospinning, and others (JAHANI; WANG; BROOKS, 2020).

Gel and sponges can encapsulate molecules in their 3D structure and complex systems like cells. For these reasons, gels and sponges are extensively used as biomedical materials like scaffolds for drug delivery, bone regeneration, 3D models for *in vitro* assays for cytotoxicity studies, and others (HAN *et al.*, 2014b, a; PARVEEN; MISRA; SAHOO, 2012).

2.3.1 - Chitosan

Chitosan is a natural and biocompatible polymer with cationic properties and soluble in acid pH. It is obtained from the deacetylation of chitin, another natural polymer that composes the skeleton structure of many species of fungi, arthropods, and nematodes (PEREIRA; MUNIZ; HSIEH, 2015). The chitin and chitosan differ by

the degree of acetylation (DA). The deacetylation of chitin, illustrated in Figure 2.1, can be obtained by some methods like alkaline hydrolysis and thermo-mechanochemical technology (YU *et al.*, 1999).

Chitin is a high crystalline fibrillar polymer due to the inter and intramolecular hydrogen bond that occurs with the acetylglucosamine (GlcNac) group. Chitin presents a high GlcNac content of 0.9 DA. But the deacetylation of chitin is hardly ever 100% so chitosan can reach less than 0.35 DA as a copolymer composed of glucosamine (GlcN) and GlcNac. The DA parameter can affect material properties like solubility, hardness, and thermal stability (Pillai et al., 2009). For this reason, the DA directly influences the solubility because as less the DA is, high the solubility is due to the decrease of secondary forces between the polymer chain.

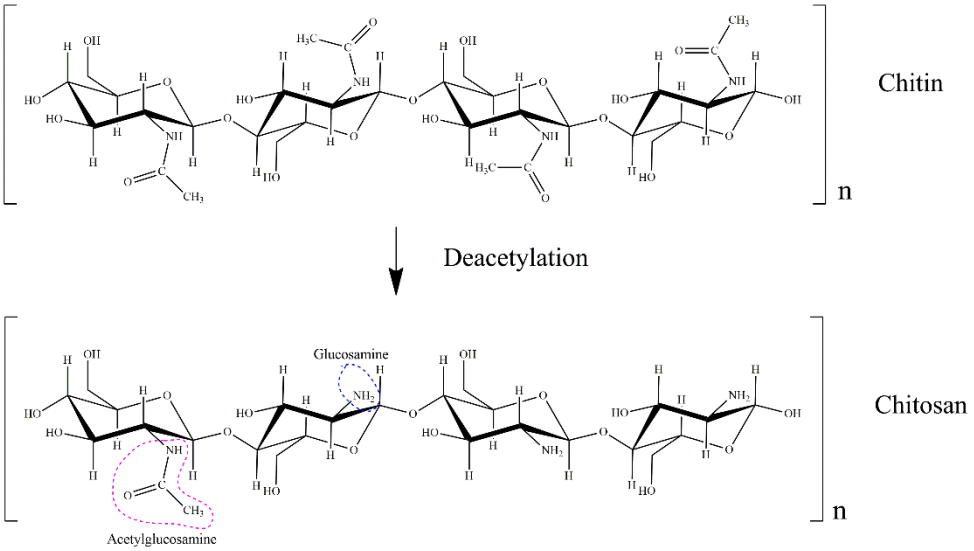

FIGURE 2. 1 - Schematic deacetylation reaction of chitin forming chitosan

The presence of GlcN in chitosan can improve the interaction of chitosan with the acid medium in which this functional group can be protonated and solubilized (PILLAI; PAUL; SHARMA, 2009). In an acid medium, liquid retention is higher than alkali, so changes in the pH can causes structural changes in chitosan, a pH-sensitive polymer (HELMLINGER *et al.*, 1997).

Swelling is the main structural change in chitosan systems Azmy et al., 2019). In lower pH and elevated temperature, the volume of chitosan can increase. In low pH, increasing protonated amine groups increase the swelling of chitosan because of the electrostatic repulsion of these groups, which decreases the mechanical properties of the polymer (ALI; AHMED, 2018). The effect of this property from the

perspective of applying chitosan as DDS is that the pH can influence the diffusion of the drug in a different medium. A higher release can occur in low pH due to the swelling release in which the electrostatic repulsion of protonated amino groups occurs. In general, the pH of the human body is very heterogeneous, in which normal tissues (subcutaneous colon) are around 7.4, the stomachal is between 1.0-2.5, stomachal cells is 6.8 and vaginal mucosa is about 3.5-4.5 (FACCHINATTO *et al.*, 2021).

Chitosan can be applied as DDS in solutions, gels, films, and sponges. Sponges and film structures usually are obtained by forming chitosan solution or gel platforms (HAN *et al.*, 2014a). After that, the material is dried by different methods like heating or freeze drying, and the final material present a dried and porous structure. Chitosan can form a gel structure by chemical or physical reticulation in which a networked material is obtained by a covalent bond or secondary interaction like hydrogen linkage.

Chitosan's chemical structure is like cellulose, so because of its strong intra and intermolecular hydrogen linkage with the hydroxyl, GlcN, and GlcNac groups, chitosan can be physically cross-linked (PILLAI; PAUL; SHARMA, 2009).

Montembault and coworkers reported a physical gelation method for chitosan based on the transition hydrophilic-hydrophobic without any chemical cross-linking or organic solvent(MONTEMBAULT; VITON; DOMARD, 2005). This mechanism is justified because chitosan is hydrophilic in acid pH but hydrophobic in an alkali medium. When chitosan acid solution is submitted to alkali conditions, a transition hydrophilic-hydrophobic occurs because the polymer's charge density is increased. In other words, the protonated glucosamine group is neutralized. They studied the gelation kinetics of chitosan and monitored different parameters. They observed that the higher the DA, the faster the gelation of chitosan because the apparent charge is increased when the DA increases, so more glucosamine groups participate in sol-gel neutralization. The neutralization leads to reducing the polymer-water interaction and forming an insoluble 3D gel structure. They also observe the influence of the polymer concentration, in which the concentration increase decreases the gelation time. After a critical concentration value, the molecular organization is so compact that the gelation occurs almost instantaneously.

The hydrophilic-hydrophobic balance generally produces a physical junction capable of forming a three-dimensional network. The final product is a solid hydrogel with a high-water content that can encapsulate molecules like drugs. This

same structure can be freeze-dried and form sponges that can well in the environment and be used for many medical applications.

2.3.2 - Poly (N-Vinylcaprolactam)

Poly (N-vinyl caprolactam) (PNVCL) is a biocompatible material obtained by the radical polymerization of the monomer N-vinyl caprolactam (Figure 2.2). Different from its monomer, PNVCL is nontoxic and can be applied as a biomaterial for many biological applications, for example, bony regeneration and drug delivery(VIHOLA *et al.*, 2005).

PNVCL is a thermoresponsive polymer that presents a sol-gel transition in a liquid medium. This characteristic is caused by a property called lower critical solution temperature (LCST). This physical-chemical property affects the solubility of the polymer in which, in temperatures above the LCST, the interactions between chain is higher than the interactions with the medium, so that the polymer forms a hydrophobic agglomerated arrange (MEDEIROS *et al.*, 2010; NOROUZI; NAZARI; MILLER, 2016; ZHU *et al.*, 2016). The polymer can encapsulate molecules inside that agglomerated structure during the sol-gel transition phase and be used as a DDS.

PNVCL presents a classical Flory-Huggins thermoresponsive behavior in water, in which the LCST decreases when the molecular weight and solution concentration are high(RAMOS; IMAZ; FORCADA, 2012). Sala et al. (2017) studied the cytotoxicity in vitro and in vivo of PNVCL with different molecular weights in bovine chondrocytes and human mesenchymal cells. They observed that the cell viability is independent of the polymer size(RL *et al.*, 2017). The practical application is the possibility to adjust this property to the final application considering the different specificities of the biological environment, and the cell viability is not affected(ZHU *et al.*, 2016).

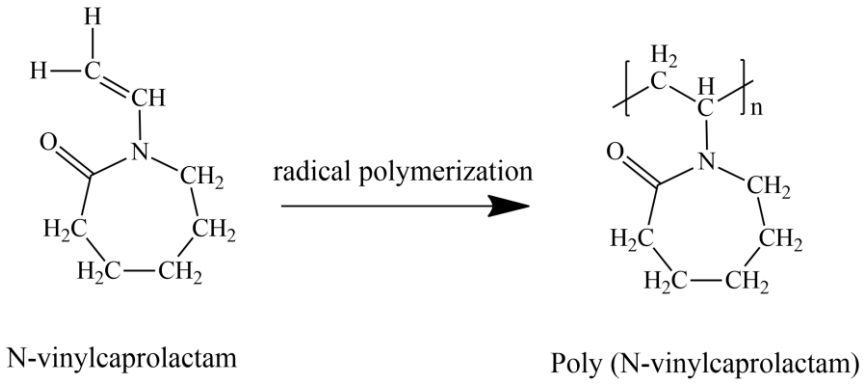

FIGURE 2. 2 - Schematic radical polymerization of PNVCL

2.3.3 - Polymeric Composites

Some studies have shown that it is possible to control many physical, chemical, and biological properties of a polymeric matrix with the insertion of nanoparticles, like changing in thermoresponsiveness, bacteria activity, mechanical properties, and biocompatibility (AK *et al.*, 2013; GAHARWAR *et al.*, 2011). In a composite, the matrix is the component that represents >50%, and the reinforcement is <50% in the material composition. The composites can contain materials such as metals, ceramics, and polymers, and the matrix and reinforcement can be from the same group of materials (ZHANG *et al.*, 2020).

Particles can reinforce ductile matrices, like polymers, but the improvement of the mechanical properties is correlated to dispersion, size, and shape. Fibers normally guarantee a better improvement of mechanical properties than particles. A non-homogeneous distribution with particles agglomerates can work as crack sites that induce the breaking of the composites under mechanical stress (GUO; POOT; GRIJPMA, 2021).

Another property that can influence the properties of the composite is the porosity. Normally non-porous materials have superior strength than porous ones with the same composition (ZHANG *et al.*, 2020). Many techniques exist to produce a porous material, like freeze-drying, electrospinning, 3D printing, etc. The porous size and strength can be adjusted to be compatible according to the final biomedical application. For example, hardiness is important for dentistry applications like prostheses to mimic the original dent (GUO; POOT; GRIJPMA, 2021). But for the development of a vaginal DDS, softness is essential to guarantee the woman's comfort. The porous materials can influence water uptake, cell migration and tissue growth.

Besides the physical-chemical characteristics, some bioactive ceramics like bioglass and silver nanoparticles can be used to improve some biological properties. Bioactive composites are materials that have the capacity to interact chemically or physically with human tissue. Bioactive composites can be applied to encapsulate and release drugs producing DDS capable of crossing biological barriers and creating a controlled release of medicines(GUO; POOT; GRIJPMA, 2021; ZHANG *et al.*, 2020).

One of the essential characteristics of applying the material as DDS is its biocompatibility in the physiological medium without generating toxic degradation products in the environment or cell death (CULVER; CLEGG; PEPPAS, 2017; HOFFMANN *et al.*, 2006; MAHINROOSTA *et al.*, 2018). Many biocompatible ceramic nanoparticles can be used as DDS or reinforce polymeric matrices like silica and magnetic nanoparticles. These ceramic materials can provide many properties to the polymeric matrix, like mechanical reinforcement, magnetic characteristics, porosity, and antimicrobial activity (HOFFMANN *et al.*, 2006; TANG; LI; CHEN, 2012).

Silica nanoparticle (SN) is a biomaterial that is largely applied as DDS. The hydrolysis of silicon alkoxides can obtain these particles in an aqueous or alcoholic medium catalyzed by acid or alkali (WU, SI-HAN; MOU; LIN, 2013). Its particle size distribution is also important for biomedical applications because the particles must cross the target tissues. Monodisperse SiO_2 can be obtained Stöber method, which is based on the hydrolysis of tetraethyl orthosilicate (TEOS) and other precursors (STÖBER; FINK; BOHN, 1968). These particles can present different sizes and shapes depending on the synthesis method. In general, using surfactants can provide structures with different porous arranges that can be very useful to encapsulate molecules (BHATTACHARYYA; WANG; DUCHEYNE, 2012).

Silica nanoparticles is involved by functional groups -OH that provide it a high surface hydrophilicity. From the perspective of a skin application, SN can encapsulate hydrophobic drugs and facilitate their permeation through the dermis and epidermis because these are the most hydrophilic skin layers (MORAIS *et al.*, 2022). Another advantage of SN is its chemical and mechanical stability under physiological conditions, not producing degradation products. SN can be classified in porous or non porous. There most common porous form is the mesoporous silica nanoparticles (MSN) that can encapsulate drugs in their porous by adsorption. Non porous SN can encapsulate drug by chemical interaction with the functional groups over silica surface.

Using SN as a DDS is promising because it is a chemically stable material, which will not generate toxic degradation products *in vivo*, it is by compatible, ease and cheap to synthesize and present form and size adjustable to obtain different release profiles.

3 - MATERIALS AND METHODS

3.1 - Materials

N-Vinylcaprolactam (NVCL, 98%, Sigmal- Aldrish, 415464), 2,2′-azobis(2-methylpropionitrile) (AIBN, DuPont, Brazil) (recrystallized in methanol for purification) and dimethyl sulfoxide (DMSO, 99.9%, Neon, 03014) were used to PNVCL synthesis. Hexadecyltrimethylammonium bromide (CTAB, 98%, Sigma-Aldrish, H5882), tetraethyl orthosilicate (TEOS, 98%, Sigma-Aldrich, 131903), 3-(trymethoxysilyl)propyl methacrylate (MPS, 98%, Sigma-Aldrish, 00901DJ-059), and ethanol (Sigma-Aldrish, 99.9%) were used to synthesize silica nanoparticles.

Chitosan high molecular weight (Ch, Sigma-Aldrish, 419416, DA=27%, MW=310000-375000 Da) and Ammonium hydroxide (30%, Neon, 01527) were used to synthesize chitosan gel and sponge. The drug release assay used clotrimazole (Thermo Scientific) and Tween 80 (Fisher bioreagents).

All other chemicals and reagents were of analytic grade or equivalent.

3.2 - Methods

The scheme bellow shows a flowchart of all the materials synthesized (Figure 3.1). The primary materials were SiO_2, PNVCL, and chitosan. The silica nanoparticles were synthesized for the alcoholic hydrolysis of a TEOS under alkali conditions. The PNVCL was obtained by radical polymerizing its monomer NVCL under an inert atmosphere. Chitosan was purchased and used without any structural modification. Chitosan was physically processed in the form of gel and sponges. The gel was obtained by a physical crosslinking by a sol-gel transition. The sponges were obtained by the freeze-drying of crosslinked gel and the freeze-drying of acetic acid chitosan solution (uncrosslinked).

The first hybrid material obtained was the PNVCL-SiO_2. This composite was obtained by the *in-situ* polymerization of PNVCL in the presence of functionalized

SiO_2. From the gel and the sponges, hybrid materials were synthesized by the direct mixture of PNVCL and PNVCL-SiO_2 inside the acetic acid chitosan solution. The sponges' composites of Ch-PNVCL and Ch-PNVCL-SiO_2

The materials were studied according to their physical, chemical, biological, pharmacological, and biomechanical properties.

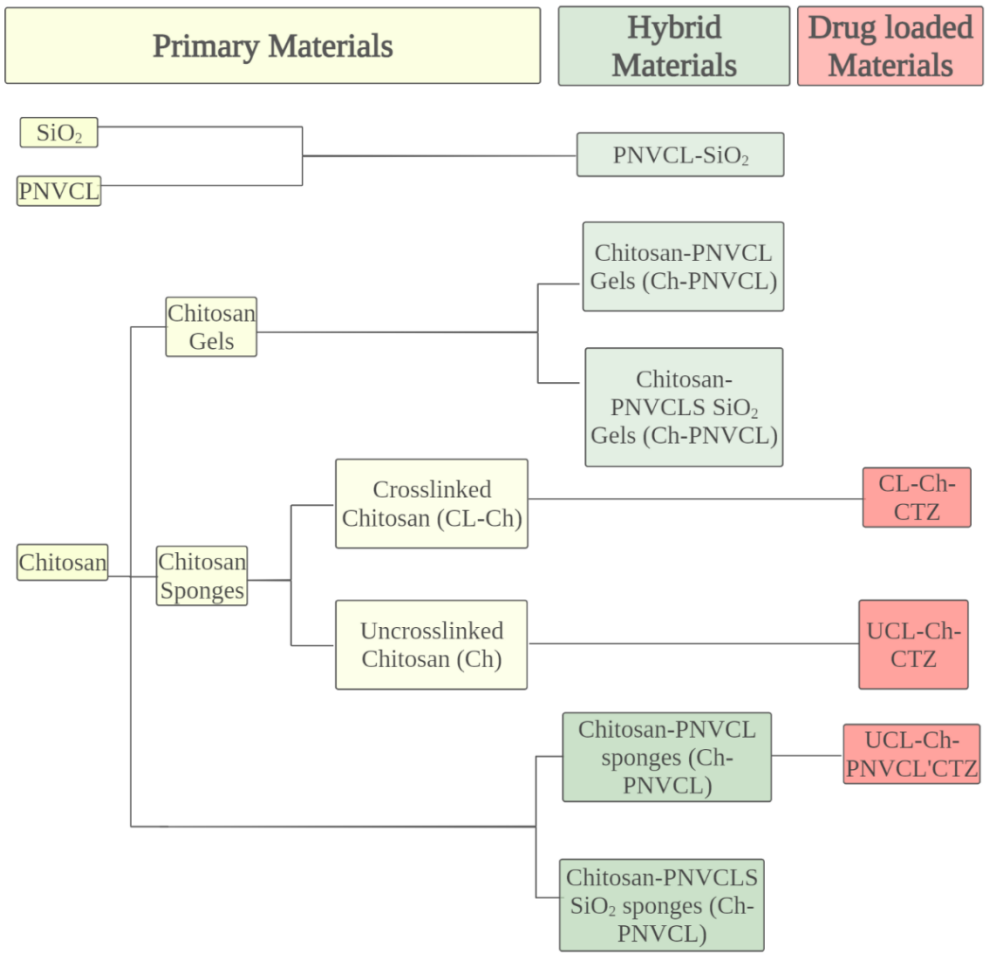

FIGURE 3. 1 - Flowchart of all the materials synthesized

3.3 - Mesoporous Silica Nanoparticles (MSN)

Mesoporous silica nanoparticles (MSN) is a biocompatible material that can present a high specific area and the possibility to control the size of the particle during the synthesis, which are promising properties to its application as a drug delivery system (WANG *et al.*, 2015). The synthesis involves the hydrolysis of silica alkoxides under an alcoholic or aqueous environment with an acid or alkali catalyst (WU, SI HAN; LIN, 2013).

For the synthesis of MSN, 3.1 mL of TEOS was hydrolyzed with 120 mL of deionized water, catalyzed by 0.9 mL of sodium hydroxide (NaOH) 2.00 M, and using 0.25 g of the surfactant CTAB. The reaction was maintained under stirring at 70^{o} C for 2 hours. After that, the material was washed until the supernatant reached pH ~7, centrifuged, and dried at 60 ^{o} C.

In this synthesis, a residual CTAB is not desirable for the final material because it can present toxicity *in vivo* in some concentrations (WAN *et al.*, 2015). So, 0.8 g of MSN was refluxed in 100 mL of methanol containing 1 mL of concentrated hydrochloric acid for 24h. The final material will be washed in ethanol and water until the supernatant reaches pH ~7, centrifuged, and dried at 70 ^{o} C.

To provide an interaction of MSN and the polymer materials in the composite synthesis, 1 g of the nanoparticles was functionalized with 10 mL MPS in 100 mL toluene for six h at 85^{o}C under stirring. The final material was centrifuged, washed with ethanol, and dried at 70^{o}C (CHEN; ZHU, 2012).

3.3 **-** Polymeric Biomaterials

3.3.1 - PNVCL

The synthesis of this polymer occurs via radical polymerization using the monomer N-vinyl caprolactam (NVCL) in the dimethyl sulfoxide (DMSO) solvent, inert atmosphere, at 70^{o} C and using the 2,2'-Azobis(isobutyronitrile) (AIBN)as radical initiator. The radical initiator will be previously purified by recrystallization in methanol.

A reactor under reflux was filled with 28 g of DMSO and 5 g of the monomer NVCL. Nitrogen was added to this mixture at 70^{o} C for 10 minutes, and then 0.13 g of AIBN was added to the reaction system. The polymerization occurred for 4 hours, and after that, the polymer was purified with several washes of deionized water using a dialysis membrane to eliminate the non-reactive materials. For the nanocomposite of PNVCL-MSN, the functionalized SiO_2 will be added to the polymerization reactor.

3.3.2 - Chitosan-PNVCL and Chitosan-PNVCL-SiO_2 Gels

The entanglement of polymeric chains forms chitosan physical hydrogel during the transition hydrophilic-hydrophobic, which decreases the polymer solution ionization and solubility, promoting hydrophobic interactions (Montembault et al., 2005). Chitosan hydrogels were prepared without any chemical cross-linking agent. Firstly, chitosan was dispersed in an acetic acid solution of 0.35 %(W/V) for 24 hours under stirring to achieve the stoichiometric protonation of the -NH_2 sites and the final concentration of 1.16% (W/V). For the hydrogel's preparation, 1.0 g of the chitosan solutions were put in a mold and transferred to a desiccator containing an ammonia bath at 30% V/V. The samples stood for 72 hours under an ammonia atmosphere, and after that time, the formed hydrogels were removed from the plates and washed several times with deionized water until the neutralization of the solution (Figure 3.2).

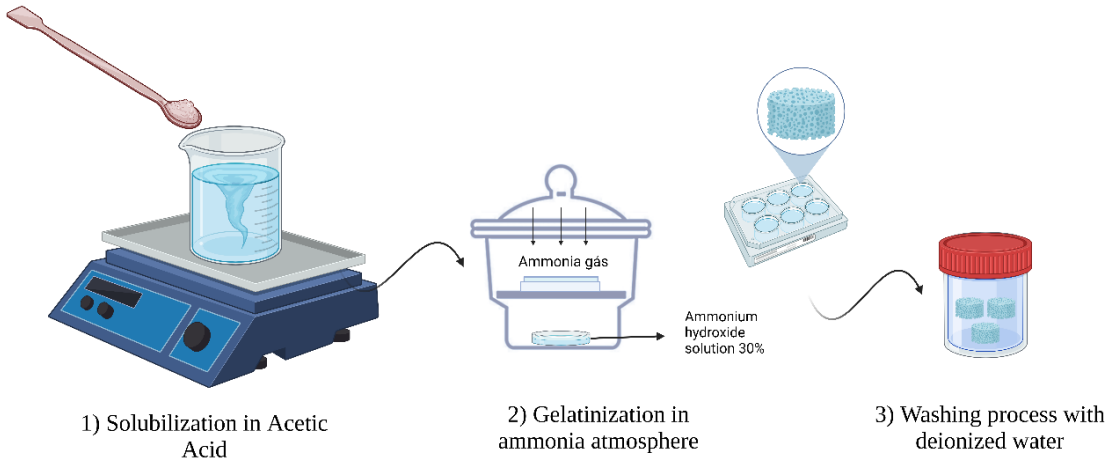

FIGURE 3. 2 - Physical reticulation method of chitosan-based materials

For the composite's synthesis, the PNVCL and PNVCL-SiO_2 were added to the acetic acid solution with a fixed quantity of chitosan to reach the final concentration of 1.16% (W/V). Firstly, we studied the concentration is summarized in Table 3.1. According to Table 3.1, chitosan is the matrix in the initial concentration (Ch-PNVCL 3:1). In the highest concentration (Ch-PNVCL 1:3), PNVCL is the matrix.

Chitosan (W)	PNVCL (W)	PNVCL-SiO_2 (W)
1	0	0
3	1	0
1	1	0
1	3	0

3	0	1
1	0	1
1	0	3

TABLE 3. 1 - Chemical and mass composition of the chitosan composites

The polymer-loaded clotrimazole (CTZ) materials were synthesized in the same way as the empty ones. The commercial concentration of CTZ in gels or creams is 1%. So, 1% solution of CTZ was prepared in acetic acid with the polymers, and the system was stirred for 24 hours. After that, the solution was placed in a mold and put under an ammonia atmosphere for physical reticulation. The gels were then washed with deionized water for neutralization.

The loading capacity (LC) and association efficiency (EE) were quantified according to the equations 10 and 11, respectively.

$$LC(\%) = \frac{\mathrm{CTZ_{recovered}}}{\text{Weight of loaded scaffold}} * 100 \quad (10)$$

$$AE(\%) = \frac{\mathrm{CTZ_{recovered}}}{CTZ_{total}} * 100 \quad (11)$$

The loaded gels were freeze-dried under -50 ^{o}C for 24 hours with the obtention of a dried sponge. The clotrimazole present in the sponge was extracted using 10 mL of DMSO under shaking for 24 hours. The extracted solution was filtered with a 0.22 µm filter and analysed by UV spectroscopy at 262 nm using a calibration curve (Appendix A).

3.3.3 - Chitosan-PNVCL and Chitosan-PNVCL-SiO_2 Sponges

The chitosan sponges were prepared by two methods: sol-gel and freeze-drying. The first one was the freeze-drying of the gels obtained by physical reticulation under an ammonia atmosphere after washing (Figure 3.3(a)). In this method, the polymer is physically crosslinked due to a hydrophilic-hydrophobic transition in which the chitosan forms insoluble entanglement. The samples were frozen for 24 hours at -20 ^{o}C and freeze-dried at -20^{o}C for 24 hours. The second method was the freeze-drying of chitosan solutions obtained after 24 hours of

solubilization (Figure 3.3(b)). The solutions were directly frozen at -20 °C and freeze-dried at -20°C for 24 hours. The same formulations described in Table 3.1 were used for both sponge syntheses. The chitosan synthetized by the gel freeze-drying will be named CL-Ch in this text, and the solution (uncrosslinked) freeze-drying will be the UCL-Ch. The drug-loaded sponges were obtained by the direct solubilization of CTZ in an acetic acid solution with the polymer. The solution was frozen for 24 hours at -20 °C and freeze-dried at -20°C for 24 hours. In this case, the association efficiency was considered equal to 100 % because neither intermediate process in the material can stimulate the elimination of the drug from the sponge.

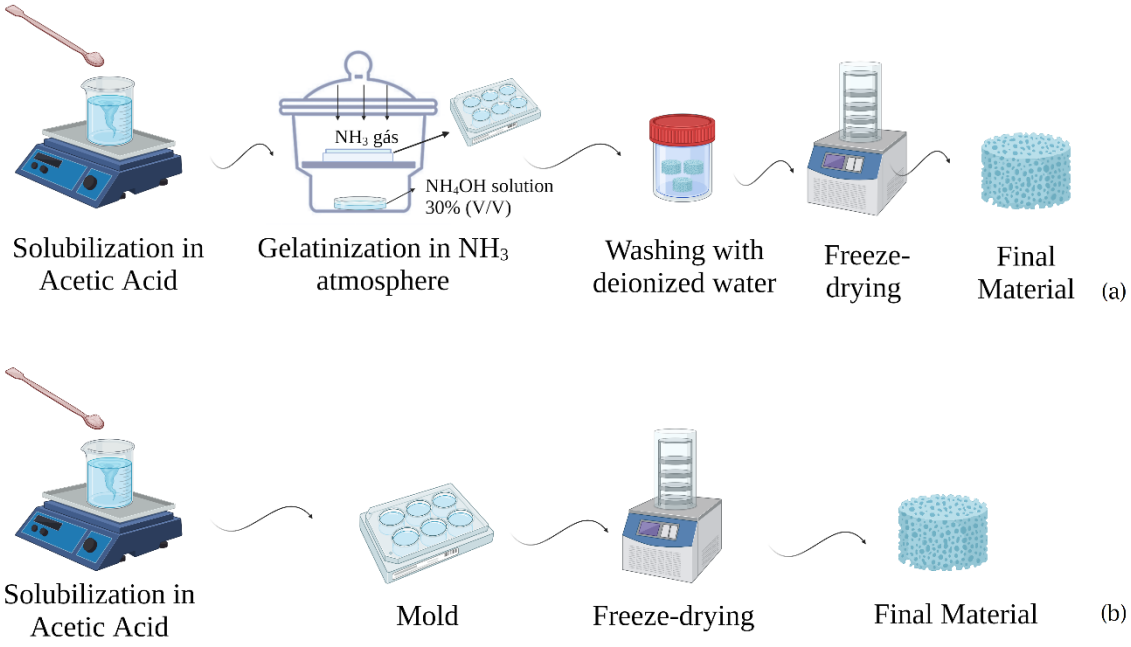

FIGURE 3. 3 - Physically crosslinked chitosan sponges (a) and Uncrosslinked chitosan sponges (b)

3.4 - Materials Characterizations

The materials were characterized according to their chemical composition, thermal analysis, rheology, morphology, texture, and antifungal activity against some *candida species*, cell viability using epithelial cell lines from the female genital tract (namely HEC-1-A endometrial cell and Ca Ski cervical cell) and the drug release assay. The gels and the sponges were studied to comprehend their potential application as a DDS in the vaginal route for the treatment of *candida*.

The morphology and chemical structure of MSN and the nanocomposites were characterized by scanning electron microscopy (SEM), Brunauer–Emmett–Teller

(BET) method, Fourier-transform infrared spectroscopy (FTIR), and nuclear magnetic resonance spectroscopy (NMR) of hydrogen. For the hydrogels analysis by SEM, the materials were previously freeze-dried. The thermal properties were characterized by differential scanning calorimetry (DSC) and thermogravimetric analysis (TGA). UV-Vis spectroscopy was used to determine the LCST of the macromolecules considering the phase transition with the temperature variation. The mechanical properties of hydrogels were studied using a rheometer to evaluate the elastic and loss modulus.

3.4.1 - Chemical Characterization

The chemical characterization of the individual materials and their composites was performed using the spectroscopy technique of Fourier-Transform Infrared (Shimadzu, IRPrestige-21), with scanning of 32, resolution 4 and in the wave number region of 400-4000 cm^{-1}. For the measurements, KBr pellets were prepared with individual materials previously dried.

For the Nuclear Magnetic Resonance of hydrogen, the PNVCL and PNVCL SiO_2 were dissolved in deuterated oxide (D_2O) at 10 mg/g for 24 hours for complete solubilization at room temperature. Chitosan was solubilized in HCl solution 0.21% in D_2O in the concentration of 10 mg/g for 24 hours at room temperature. The ^1H NMR was performed in a Bruker Avance III spectrometer that operated in a magnetic field Oxford of 9.5 Tesla, that has corresponding frequency of 400 MHz for the hydrogen-1 nucleus.

3.4.2 - Thermal Analysis

The main thermal property of PNVCL in the perspective of biological characterization is the Lower Critical Solution Temperature, a physical-chemical phenomenon in which the interaction polymer-polymer is superior to its interaction with aqueous media. Consequently, the polymer changes from a soluble specie to an agglomerated form above LCST (ZHU *et al.*, 2016). This property was studied by the variation of the light optical density and transmittance of a polymeric solution of PNVCL and PNVCL-SiO_2 with the temperature from 30 to 50 ^oC in the spectrum change of 233-800 nm. The polymeric solution was maintained for 3 minutes under each temperature to reach the thermal equilibrium before the measurements. For the evaluation of the effect of the polymer concentration in the LCST and also the impact

of the silica nanoparticles, the polymeric solutions with 3%, 2%, 1%, 0.5%, and 0.1% of PNVCL and PNVCL-SiO_2 were analyzed with the variation of the temperature from 25 to 50 ^oC at the wave length of 500 nm. In absorbance mode, these measurements were performed in a Synergy Mx microplate reader (Biotec).

The TGA was performed in a thermogravimetric analyzer TGA (NETZSCH STA 409C) at a heating hate of 10 ^oC/min using an argon flow of 50 mL/min in an aluminum crucible.

The DSC of the materials was performed to determine the glass transition temperature (Tg) of the materials using a differential scanning calorimeter (DSC 204 Phoenix, Netzsch, Germany). The samples were placed in an aluminum crucible and analyzed at a 10 ^oC/min heating rate with 60 mL/min nitrogen flux for two heating cycles.

3.4.3 - Rheology

The rheology study of the chitosan, PNVCL, and its composites was performed using the kinexus rheometer (Malvern), in which the viscosity of the solution and the oscillation analysis of the gels were studied. The viscosity assays were performed in the shear range from 0.01 to 100 $^{-1}$ at 37^o C using an upper cone plate CP4 (40 mm) with 4 degrees, a lower plate PLS55 (55 mm), and 1.2 mL of polymeric solution.

Oscillatory measurements were performed at 1 Hz in the shear range of 0.01%-500% at 37 ^oC to determine the linear viscoelastic zone (LVE), the region in which the shear strain does not affect the structure of the materials because the shear strain is constant.

3.4.4 - Morphology and Texture Analysis

The morphological characterization of the materials was performed using a field emission gun scanning electron microscopy (FEG-SEM) Supra 35-VP (Carl Zeiss, Germany). The SiO_2 was previously dispersed in water, deposited in a silicon substrate, and analyzed with the accelerating voltage of 5.00 kV. The Chitosan and PNVCL composites were previously freeze-dried, deposited in the carbon substrate, and analyzed with the accelerating voltage of 1.00 kV.

The liquid displacement method determined the sponges' porosity and density(Han et al., 2014b). Previously, the volume of the scaffolds (V_{sc}) was measured using the diameter height. Ethanol was used as displacement liquid because it can permeate the scaffold without swelling. The dried sponge was precisely weighed (W_1) and placed in a volumetric cylinder containing a known volume of ethanol (V_1) for a specific time at room temperature to allow solvent permeation.

The solvent volume impregnated in the polymer (V_s) was also determined by the weigh difference between the solvent-impregnated scaffold (W_2) and the dried one, divided by the solvent density, according to the equation 12.

$$V_s=(W_2-W_1)/\rho \qquad (12)$$

According to these measurements, the porosity was determined by the equation 13.

$$P=V_s/V_{sc}*100 \qquad (13)$$

The density was also determined according to the equation 14.

$$d=W_1/V_{sc} \qquad (14)$$

The Ch-PNVCL sponges composites obtained by the solution freeze-drying method and chitosan obtained by the crosslinking method were evaluated according to the hardness using the compressive test in a texturometer. Samples of chitosan sponges containing different concentrations (W/W) of PNVCL were compressed up to 80% of their original length at the compressive rate of 1.2 mm min^{-1} and 0.5 N of force. Considering the application as a DDS for vaginal mucosa, compressive stress is an important parameter to evaluate the materials' comfort.

Textural analysis of pure and functionalized mesoporous silica was evaluated by the technique of adsorption and desorption of N_2 in the equipment Micromeritic (ASAP 2020). The analysis was carried out at -186 ^oC using N_2 as an adsorbent. The specific area was calculated by Brunauer–Emmett–Teller (BET) method in low relative pressure (p/po=0.00-1.00).

3. 4.5 **-** Biopharmaceutical and biological properties of Sponges

3.4.5.1 **-** Antifungal Microdilution Broth Assay

Clotrimazole and the materials loaded with clotrimazole were tested for different *candida* species according to the CLSI protocol M27. Because clotrimazole is an insoluble molecule, the assay was performed using 1% of dimethyl sulfoxide (DMSO) as an intermediate solvent in the RPMI medium. The pure clotrimazole was dissolved in DMSO at 100 x the highest concentration of the assay. In that concentration, DMSO does not cause mortality of *candida* species. The clotrimazole was extracted with DMSO from the sponges, and the extract concentration was also adjusted to 100 x the test concentration. The CTZ was extracted from the sponges for 24 hours using an extractant volume considering the sample area of 3 cm^2/mL according to the recommendations of ISO 10993-12 for sample preparation and reference materials (INTERNATIONAL ORGANIZATION FOR STANDARDIZATION, 2012).

For this assay, candida's species were firstly seeded in a medium Sabouraud Dextrose Agar (SDA) for 24 hours at 37^o C. After the growth, the inoculum is prepared by picking colonies of *candida* species and suspended in 5 mL of sterile 0.145 mol/L saline (8.5 g/L NaCl; 0.85% saline) and adjusting the cell concentration for 5,0 x 10^2 - 2,5 x 10^3 cell/mL.

The specie was placed in RPMI and incubated in a 96 wells plate with different concentrations of clotrimazole for 48 hours at 37 ^{o}C. After 48 hours, the plate was analyzed in a microscope to determine the minimum inhibition concentration (MIC) and the minimum fungicide concentration (MFC). The MIC is the minimal concentration capable of limiting the growth of the fungi, while the MFC is the lowest concentration, capable of killing at least 99% of the inoculum (FACCHINATTO *et al.*, 2021).

The results obtained for the antifungal susceptibility, according to the azole resistance profile, were classified as susceptible (S; MIC≤8μg mL-1), dose-dependent susceptibility (SDD; MIC=16-32 μg mL-1) and resistant (R; MIC≥64 μg mL-1).

The *candida's* species tested were *C. albicans* ATCC 90028, *C. albicans* ATCC 64550, *C. albicans* SC5314, *C. krusei* ATCC 6258, *C. tropicalis* ATCC 750 and *C. glabrata* ATCC 2001.

3.4.5.2 - Antifungal Disc diffusion Assay

Disk diffusion testing was performed according to the CLSI protocol M44. Petri dishes (150-mm-diameter) containing Mueller-Hinton agar supplemented with 2% glucose and 0.5 µg/mL methylene blue were used. The discs (9 mm in diameter) were charged with 25 µg of clotrimazole, 25 µg de fluconazole, and 4.5 mg of clotrimazole. 4.5 mg is the quantity of clotrimazole in the chitosan sponges with approximately 9 mm in diameter.

A sterile swab was dipped in a yeast stock suspension of 1 x 10^6 to 5 x 10^6 cells per mL of Candida species isolates to inoculate the agar plate. The discs and the sponges were subsequently incubated at 37°C for 48 hours. The zone diameter endpoints were read at 100% growth inhibition.

The *candida's* species tested were *C. albicans* ATCC 90028, *C. albicans* ATCC 64550, *C. albicans* SC5314, *C. krusei* ATCC 6258, *C. tropicalis* ATCC 750 and *C. glabrata* ATCC 2001.

We also performed the water uptake of charged sponges and disk with 4.5 mg of drug to evaluate the diffusion mechanism of drug delivery under the agar surface. For these experiments, the sterile swab was dipped in pure NaCl (8.5 g L-1) as well as performed to the assay with candida. After that, pre weighed (W1) discs and sponges were placed in the petri dish and incubated for 48 hours at 37 o C. After this time, the materials were weighed again (W2), and the water uptake was calculated according to the equation 15.

$$Wt = \frac{W_2 - W_1}{W_1} * 100 \qquad (15)$$

3.4.5.3 - Cell Viability

The resazurin method was used to evaluate the cell viability evaluation. It consists of measuring the metabolic capacity of live cells in the presence of possible cytotoxic agents. The resazurin (blue color) is oxidized to the resofurin (pink) by the mitochondrial respiratory chain in cell lines. So, the quantity of resofurin is proportional to the number of live cells.

The *in vitro* cell viability was performed to evaluate the safety of the materials in the physiological environment. Ca Ski and Hec-1-A epithelial cell lines, both from ATCC (Manassas, VA, USA) chosen as models due to their presence in the human uterus, cervix, and endometrium. These models have relevance to predicting if vaginal safety will be maintained with the insertion of the chitosan sponges. These cell lines were maintained in RPMI 1640 medium (Ca Ski) and McCoy's 5A medium (Hec-1-A), both supplemented with 10% (v/v) fetal bovine serum, 100 U mL^{-1} penicillin and 100 µg mL^{-1} streptomycin under standard cell culture conditions (37 °C, 95% RH and 5% CO_2). The medium was changed each 2-3 days to allow cell growth.

The materials were previous submitted to an extraction with the specific medium to each cell line. The extraction was performed using the ratio of 3 cm2 mL -1 at 37 oC for 24 hours as recommended by ISO 10993-12.

Each cell line was incubated in 96 well plates in the concentration of 5000 cells per well for 24 hours in its respective medium. After this time, each well had its medium removed and washed with phosphate-saline buffer (PBS) to remove the death cells. After that, for the positive control (alive cell), 200 µL of the medium with the cells was used. For negative control (death cells), 1%(v/v) triton-X in the supplemented medium, and for the background, supplemented medium without the cells. For the biocompatible evaluation, 200 µL of each empty and drug-loaded extract was placed in the 96-well plate with the controls. The plate was again incubated under routine cell culture conditions for 24 hours.

After this time, the cells were washed with 200 µL of PBS, and after that, each well was filled with 200 µL of resazurin solution 10 % in supplemented medium (V/V) and incubated again for 2 hours in the dark at 37 oC. After that, 100 µL of each well was transferred to a black-walled transparent-bottom 96-well plate and analyzed at fluorescence λem=530 nm, λex=590 nm.

The cell viability was calculated according to the fluorescence values following the equation 16. All the experiments had six replicates.

$$Cell\ viability\ \ (\%) = \frac{experimental\ value - dead\ cells\ control}{live\ cells\ control - dead\ cells\ control} \times 100 \qquad (16)$$

3.4.5.4 - Drug Delivery

The drug delivery assay for hydrophobic molecules like clotrimazole can be a challenge due to its low solubility in the aqueous medium. The condition of this assay must mimic the environment of the place where the drug will be delivery. For this reason, before performing the clotrimazole drug release, the sink conditions were adjusted. The sink condition is the capacity of a medium to solubilize at least three times the amount of a drug. The solubility of clotrimazole in aqueous medium is very poor. So that isn't very easy to simulate a drug delivery, considering that the physiological medium is formed mainly by water.

The vaginal fluid simulant (VFS) was chosen for the drug delivery assay to simulate a healthy vaginal environment with a pH of around 3.5-4.5. The VFS was prepared with 3.51 g of sodium chloride, 1.4 g of potassium hydroxide, 0.222 g of calcium hydroxide, 2.0 g of lactic acid, 1.00 g of glacial acetic acid, 0.16 g of glycerine, 0.4 g of urea, and 5.0 g of glucose. The reactants were solubilized with 900 mL of deionized water, and after the pH adjustment to 4.2, the volume was completed for 1 L.

The solubility of clotrimazole was determined in 7 different conditions: in pure VFS, and VFS with different concentrations of two surfactants – poloxamer 407 and Tween 80 (1, 2, 2pm. After this time, the sample was filtered and analyzed by UV spectroscopy at 262 nm using a calibration curve.

After the solubility tests, the drug delivery assay was performed with chitosan sponges synthesized for the crosslinked and uncrosslinked methods (See Figure 3.3). For VFS, the sponges were incubated in 50 mL of a pre-heated medium at 37 oC under shaking of 50 rpm, and 1 mL of medium was collected and replaced with fresh medium at the set points of 0.25, 0.5, 1, 2, 4, 8 and 24 hours. In order to understand better the drug release mechanisms, the drug release profiles were modelled and fitted according to the kinetic laws zero order, first order, Higuchi, Hixson-Crowell, Ritger-Peppas and Weibull.

4 - RESULTS AND DISCUSSION

4.1 - SiO_2

The alkaline hydrolysis of TEOS synthesized the SiO_2. In this reaction, the silica precursor is hydrolyzed with the substitution of ethyl groups by water forming a hydrated silica tetrahedron. In the second step, these molecules are condensed to form a tridimensional Si-O-Si structure according to equation 17. A mesoporous silica can be achieved using surfactant molecules acting as structure-directing agents, normally long-chain alkyl trimethylammonium halides.

$$nSi\text{-}OR4 + 4H_2O \rightarrow nSi\text{-}(OH)_4 + n4ROH \rightarrow (SiO_2)n + ½nH2O \quad (17)$$

Figure 4.1 shows the FT-IR spectra of the SiO_2 nanoparticles. The synthesized SiO_2 presented bands in the range of 3700-3200 related to -OH groups in the material's surface and the 830-1110 cm^{-1} associated with Si-O characteristics of the silica nanoparticles. The bands of 1452, 2850, and 2925 cm^{-1} corresponding to the CH_2 deformation plane, symmetric stretch, and asymmetric stretch, respectively, are related to the presence of the surfactant CTAB present in the SiO_2-CTAB spectra. After washing, all the CH_2 bands disappeared, confirming the removal of surfactant in the SiO_2.

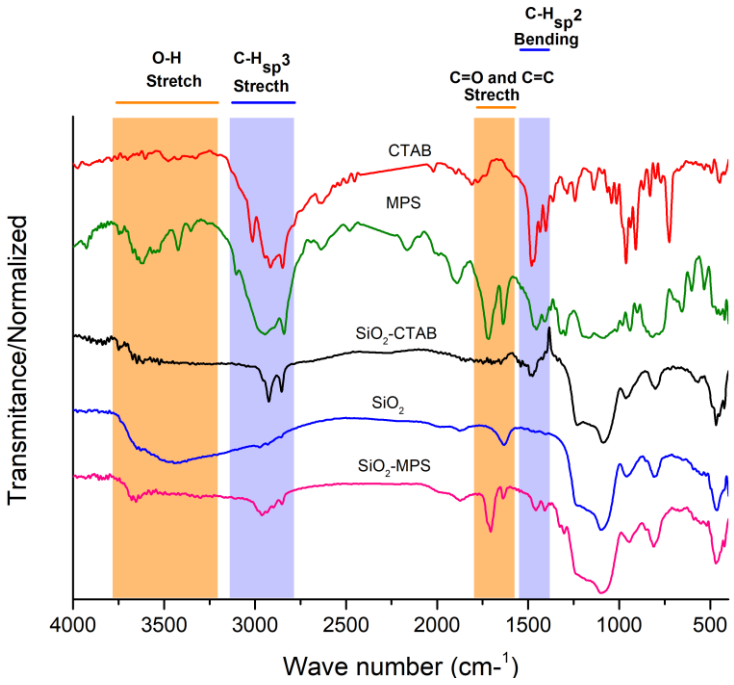

FIGURE 4. 1 - Superficial modifications of mesoporous SiO_2

After the MPS functionalization, new bands appeared in the SiO_2-MPS spectra. The band at 2835 cm^{-1} and the range of 1462-1300 cm^{-1} correspond to the asymmetric stretch of CH_2, and CH_2 deformation on and out of the plan, respectively, also present in the SiO_2-CTAB spectra. The picks at 1710 and 1641 cm^{-1} are related to the stretch of C=O, and C=O and C=C conjugation, typical of the ether group. This indicates that the functionalization of SiO_2 and the MPS was effective.

Silica nanoparticles are porous spheres with an average diameter of 150 nm and a polydispersity index (PdI) of 0.02, indicating that the material is monodisperse (Figure 4.2 a and b). This index is obtained by the square standard deviation divided by the average diameter, and the samples are considered monodisperse when PdI is less than 0.1. The gap in the nanoparticles is caused by the surfactant CTAB. Before adding the precursor, the CTAB forms micelles in the alkaline solution, and the head cationic quaternary ammonium interacts with the inorganic precursor TEOS negatively charged. After the surface modification with MPS, no significant differences between the average diameter and PdI were also 0.02 (Figure 4.2 c and d). The post-synthetic functionalization process can cause an increase in pore occupation if the organosilanes react preferentially at pore opening. Using a

mesoporous SiO_2, the organosilane can occupy a high surface area that can enhance the interaction with the polymer chain for the composite synthesis.

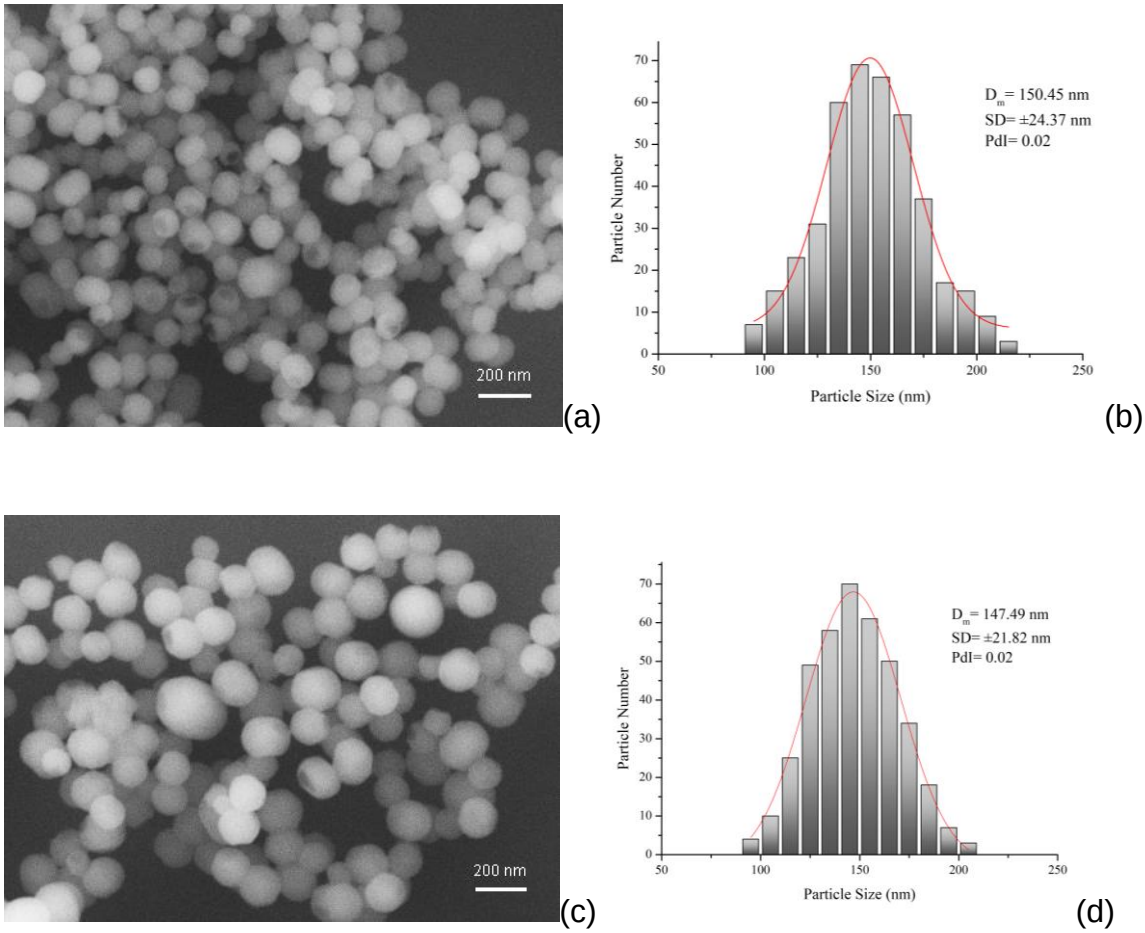

FIGURE 4. 2-Micrograph of SiO_2 nanoparticles before the superficial modification (a) and its histogram (b). Micrograph of SiO_2 nanoparticles functionalized with MPS (c) and its histogram (d).

The textural properties of the nanoparticles were investigated using the BET method (Figure 4.3). The SiO_2 and SiO_2-MPS nanoparticles present a type IV isotherm typical of mesoporous materials. The step between 0.3 and 0.4 P/P0 indicates the presence of a well-defined mesoporous structure, which is also present in the SiO_2-MPS. Type H3 hysteresis occurs due to the condensation of N_2 in the mesoporous structure. We can also observe a reduction of the quantity adsorbed, which is associated with the surface functionalization of the nanoparticles with the MPS. After the functionalization, the surface area decreased from 425.7 to 255.2 m^2g^{-1} in SiO_2-MPS. Consequently, the pore volume reduces from 0.43 to 0.22 cm^3/g. This

phenomenon is common, and it usually depends on factors like the size of the surfactant molecule and the degree of occupation of it.

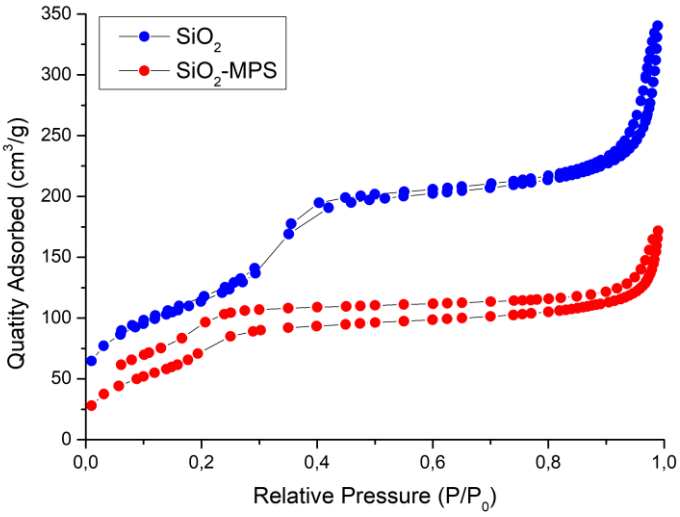

FIGURE 4. 3- Adsorption and desorption of SiO_2 and SiO_2-MPS

Sample	BET surface area (m^2g^{-1})	Pore Diameter (nm)	Pore Volume (cm^3/g)
Pure SiO_2	425.70	4.04	0.43
SiO_2-MPS	255.21	3.59	0.22

TABLE 4. 1 - Textural parameters of silica nanoparticles

4.2 - PNVCL and PNVCL-SiO_2

To evaluate the NVCL polymerization, we used the FTIR analysis of the main functional groups of studied materials (Figure 4.4). The band at 3108 cm^{-1} is associated with the stretching of the C-H bond sp^2 in the vinyl group (=C–H) on NVCL spectra. At 1668 and 1630 $cm^{-1,}$ the stretch bands represent the C=C and C=O, respectively, on NVCL spectra. The disappearance of bands C=C and C-H bond sp^2 on PNVCL and PNVCL-SiO_2 characterize the conversion of the monomer in the polymer. The bands CH_3 sp^3 symmetric and asymmetric, carbonyl C=O, and C-N

stretching from the bond -N-$(CH_2)_2$, at 2933, 2836, 1630, and 1200 cm^{-1} are maintained on PNVCL and PNVCL-SiO_2. On PNVCL-SiO_2, it is possible to see an enlargement of the band 1088 cm^{-1} compared to the PNVCL spectra. This peak's overlap with the asymmetric stretch of Si-O-Si and 1105 cm^{-1} characterize the presence of silica nanoparticles at the polymeric structure.

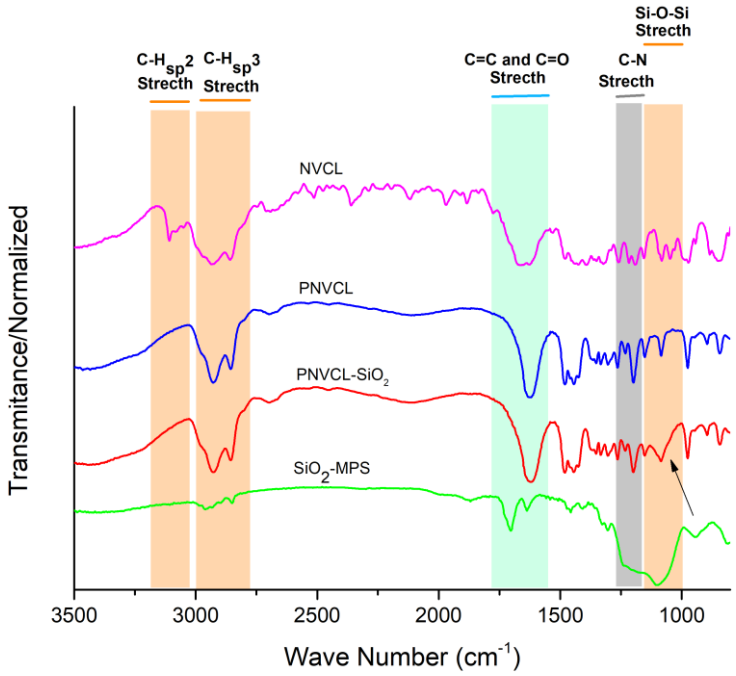

FIGURE 4. 4- FTIR spectra of the NVCL, PNVCL, PNVCL-SiO_2, and SiO_2-MPS.

We also evaluated the polymerization of NVCL by NMR spectroscopy. Figure 4.5 presents the NMR spectra of the monomer and its derivatives. The three methyl groups (H_a) in the caprolactam ring are equivalent and appear at 1.53-1.71 ppm. The hydrogens H_b and H_c near the carbonyl group have peaks at 2.57 and 3.62 ppm. The three protons (d, e, and f) in the vinyl group (C=C) presented chemical shifts at 4.56, 4.73, and 7.07 ppm. The last peak has a higher chemical shift due to its position concerning the oxygen and nitrogen atoms. The disappearance of this peak is an indicator of polymerization of the NVCL, in which the chemical bond C=C is broken. The PNVCL and the PNVCL-SiO_2 presented four characteristic peaks of chemical shifts. The proton H_a of the caprolactam ring is broader than in the NVCL.

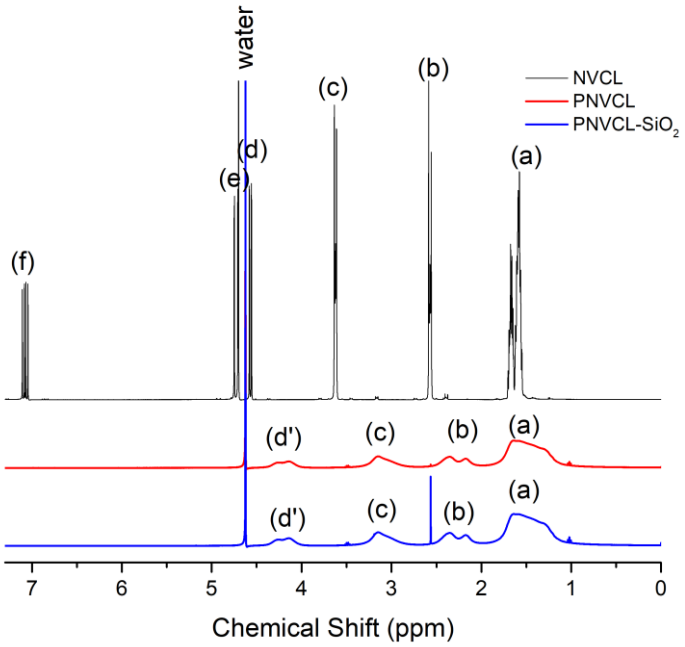

FIGURE 4. 5-NMR spectra of NVCL, PNVCL, and PNVCL-SiO_2

The LCST is a solution property based on the transition hydrophilic-hydrophobic in water. Under the LCST, the hydrophilic interactions with water are superior to the polymer chain interactions, so the macromolecule presents a coil form (Figure 4.6(a)). When the solution reaches the LCST, the polymer chain interaction is superior to the water interaction, so the hydrophobic interaction leads the polymer to a globule form. That phase transition presents several influences on the system, for example, the changes in the solution's optical properties from a transparent to an opaque solution (Figure 4.6(b)). This property is very interesting from the perspective of its application in biomedicine because the globule phase can encapsulate and protect molecules for its application as a drug delivery system.

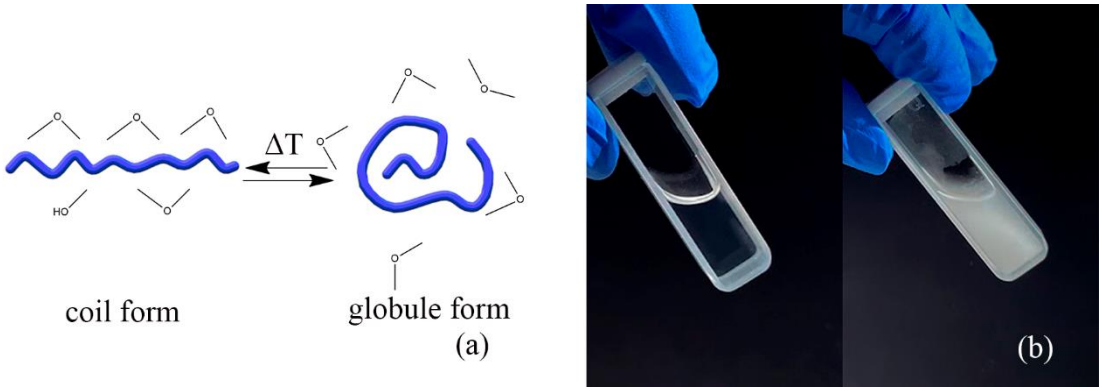

FIGURE 4. 6-Scheme of the phase transition of the coil to globule form in the LCST (a) and the macroscopic aspect of the polymeric solution under these two states (b)

The LCST of PNVCL and PNVCL-SiO_2 was investigated by spectroscopy by the change in the optical properties of the polymeric solution over the temperature variation. Figure 4.7 shows the graph of transmittance vs. wavelength in a temperature range from 30 to 50 ^oC. It is possible to observe an abrupt decrease of transmittance when the temperature reaches 35 ^{o} C that characterizes the LCST of PNVCL (Figure 4.7(a)). During the 36-50 ^oC range, the transmittance tends to zero because the globule state is predominant in the polymeric solution.

The same data for PNVCL-SiO_2 shows a profile in which the transmittance of the solution tends to decrease with the decrease of the wavelength due to the presence of the nanoparticles (Figure 4.7(b)). In smaller wavelengths, the transmittance is reduced because the wavelength (~233-400 nm) is very similar to the size order of silica nanoparticles (~150 nm). At this wavelength range, an elastic scattering effect decreases the transmittance of the polymeric solution of PNVCL-SiO_2. The impact of the elastic scattering of SiO_2 is combined with the globule conformation of the polymer when the temperature reaches 35 ^{o} C, in which the transmittance declines to ~0-7% over the range of 233-800 nm. However, from 38 ^{o} C, the transmittance increases. This increase suggests that the nanoparticles favor the polymeric interaction with water and enhance hydrophilic interactions at certain temperature points.

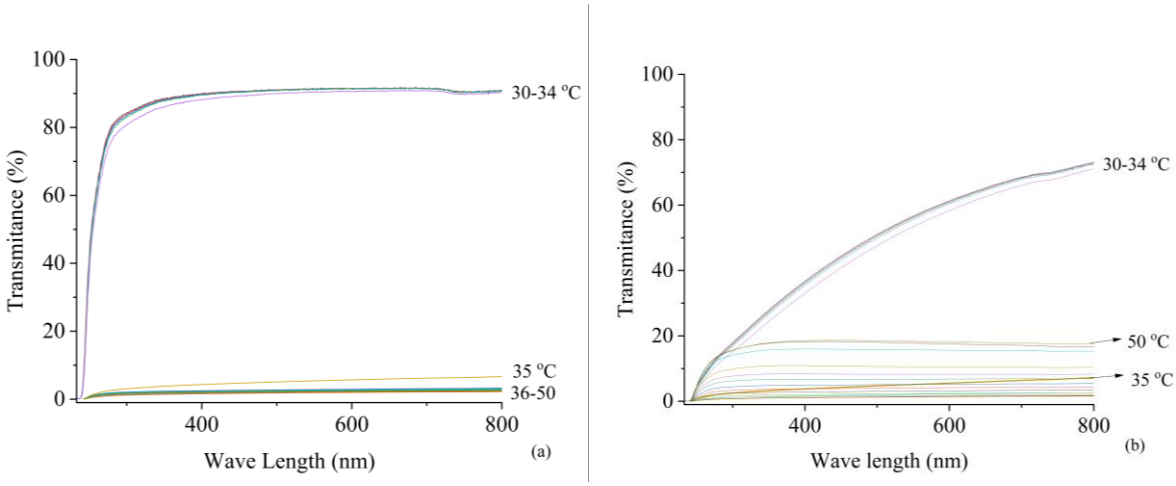

FIGURE 4. 7-Scanning of the change of transmittance from 233-800 nm with the temperature variation for PNVCL (a) and PNVCL-SiO_2 (b)

PNVCL presents a Flory-Huggins thermoresponsive effect that can vary with the polymer chain size and the concentration of the polymeric solution in water. At higher concentrations and polymer chain size, the phase transition from the coil state to the globule state tends to occur at lower values of temperatures (See Figure 4.6 a and b). The polymer concentration effect was studied with five solutions (3%, 2%, 1%, 0.5%, and 0.1%) at the wavelength of 500 nm with the variation of the temperature from 30-50 ^{o} C for PNVCL and PNVCL-SiO_2 (Figure 4.8 a and b). At the studied range, a variation of LCST of 2 degrees in the 0.1% solution was observed compared to the 1, 2, and 3% (Table 4.2). Higher energy is required to induce the phase transition at low concentrations. This phenomenon happened because the polymer chains are more dispersed in an aqueous solution at low concentrations, so more energy is necessary to favor the molecule aggregation.

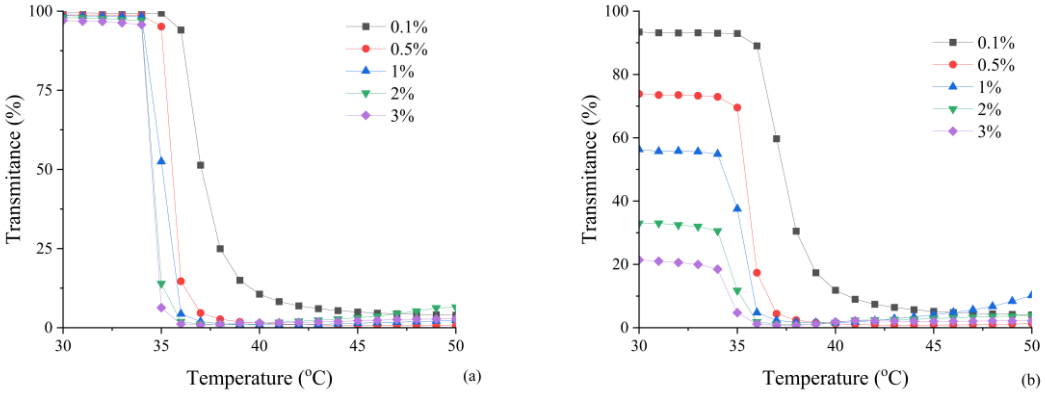

FIGURE 4. 8-Effect of concentration on values of LCST of PNVCL (a) and PNVCL-SiO_2 (b)

Concentration (%)	Materials	Onset	LCST
0.1	PNVCL	35	36
	PNVCL-SiO_2	35	36
0.5	PNVCL	34	35
	PNVCL-SiO_2	34	35
1	PNVCL	34	34
	PNVCL-SiO_2	34	35
2	PNVCL	34	34
	PNVCL-SiO_2	34	34

3	PNVCL	34	34
	PNVCL-SiO_2	34	34

TABLE 4. 2 - Values of LCST at different concentrations

The thermogravimetric analysis was used to determine the degradation events of the polymers. Figure 4.9 shows a little mass loss of about 5% until 370 ^{o} C due to absorbed moisture. There is a difference of about 1% of mass between the materials in which PNVCL-SiO_2 can retain more humidity than PNVCL. There is a significant mass loss at 400^{o} C and 465 ^{o} C due to the degradation of PNVCL. After that temperature, there is a formation of an intermediate compound with thermal stability from 465 to 520 ^{o}C that can be attributed to the opening of the caprolactam ring with the formation of nylon 6. Around 620 ^{o}C, the degradation of the organic phase is complete, and there is the remaining SiO_2 without the presence of water and MPS. The exact percentage of SiO_2 in the PNVCL structure is 3.85%, estimated by the mass difference between PNVCL and PNVCL-SiO_2 after the polymer degradation.

The PNVCL is classified as an amorphous biopolymer that has a random molecular arrangement with a rigidity of a solid. The glass temperature (Tg) is a thermal transition event in which a polymer changes from a vitreous state to a viscous state. The Tg value does not change with the insertion of silica nanoparticles, which means that the mobility of the polymer chain is not affected. So, the molecular mobility is reduced below the Tg, an attractive characteristic in the perspective of controlled drug delivery because the diffusion of molecules is reduced (Cortez-Lemus & Licea-Claverie, 2016).

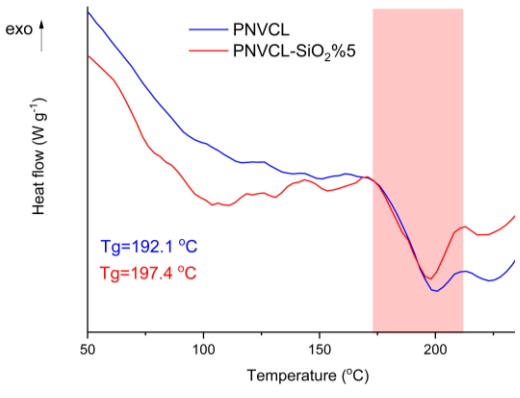

(a) (b)

FIGURE 4. 9-Thermal analysis of PNVCL and PNVCL-SiO_2. (a) Thermogravimetric analysis, (b) Differential Scanning Calorimetry

4.3 - Chitosan-PNVCL/SiO_2

Chitosan is a polymer derived from the deacetylation of chitin, a polysaccharide obtained from the skeleton structure of many species of fungi, arthropods, and nematodes (PEREIRA; MUNIZ; HSIEH, 2015). Figure 4.10 shows the H1 NMR spectra of the commercial chitosan. The chemical shift in 4.7 ppm corresponds to the H_a linked to the anomeric carbon C1. The hydrogens bonded to C3-C6 (H_b) present a similar chemical environment, so its signals overlap in 3.2-4.0 ppm. The signal in 2.9 ppm is relative to the hydrogens bonded to the C2 (H_c) with the same chemical environment in the presence of GlcN or GlcNac in the soluble medium.

In some cases, the NRM spectra can present different signals for ClcN (H2) and for ClcNac (H2') when the chitosan or chitin are not solvated in the aqueous medium. Hydrogens bonded to the methyl carbon (H_d) in the GlcNac group appear at 1.98 ppm. Using NMR spectroscopy is possible to obtain the DA of acetylation of chitosan.

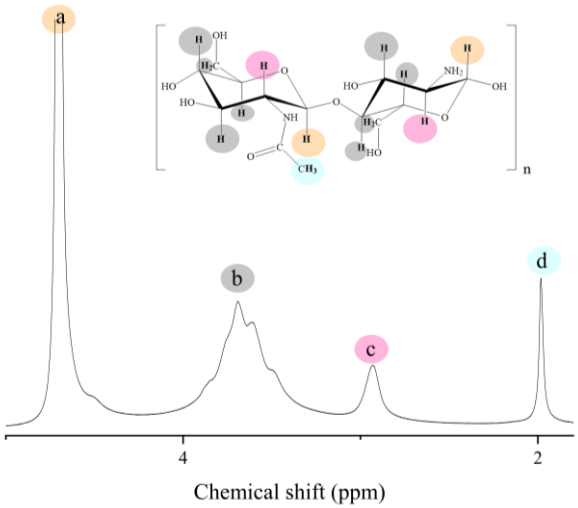

FIGURE 4. 10-NMR of chitosan

The DA can be estimated by integrating the methyl H_d in the GlcNac group and the H_c in the C2 according to equation 18.

$$DA = \frac{\frac{1}{3} * ICH_3}{IH2 + IH2'} \qquad (18)$$

Where ICH_3 is the integral of the hydrogens in the GlcNac group (H_d), and the IH2 is the integral of the chemical shift of hydrogens bonded to GlcN and IH2' is when the hydrogen is bonded to GlcNac. For this work, we used just the integral of signal Hc because these hydrogens present the same chemical shift. The %DA was 0.26, which indicates a chitosan composition. Chitosan with a lower %DA can be associated with poor solubility in aqueous medium.

The physical association of chitosan and PNVCL using the physical crosslinking was evaluated using the FTIR of the freeze-dried gels (Figure 4.11). The main vibrational fingerprint of chitosan are the bands at 1644 cm^{-1} C=O stretch characteristic of acetylglucosamine group (amide I), 1564 cm^{-1} a mixed N-H and C-N stretch of secondary amides N-H (amide II) and C-O-C bridge that is characteristic of polysaccharides at 1152 cm^{-1}. As previously discussed, the principal PNVCL bands

are carbonyl C=O and C-N stretch from the bond -N-$(CH_2)_2$ at 1200 cm^{-1}, maintained on PNVCL and PNVCL-SiO_2. According to Figure 4.11, neither PNVCL nor PNVCL-SiO_2 were effectively associated with chitosan structure because after the analyses of the normalized spectrum, it was impossible to observe the appearance of PNVCL bands in the blends or increasing of bands in common like C=O stretch. This behavior is explained because PNVCL is soluble in water at room temperature, in which the washing process of the gels was performed. The PNVCL and PNVCL-SiO_2 were solubilized and removed from the chitosan structure during the washing process.

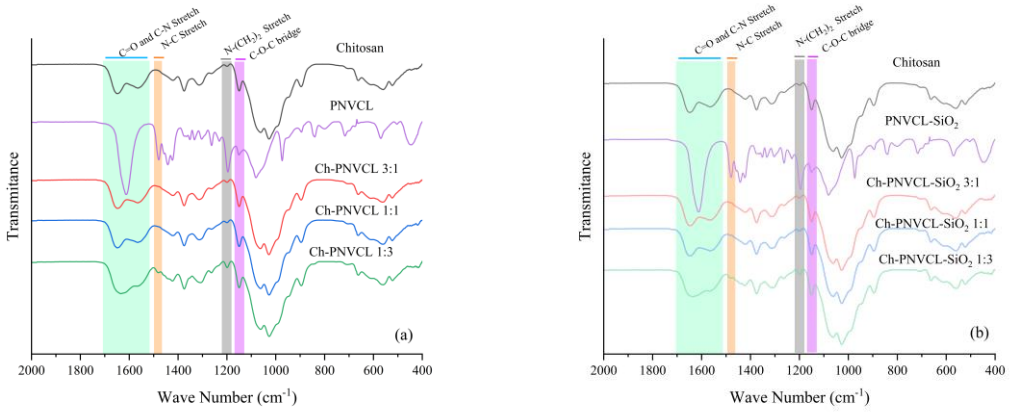

FIGURE 4. 11-FTIR of chitosan-PNVCL (a) and chitosan-PNVCL-SiO_2 (b) hybrid materials obtained by freeze-dried gel

Although the physical association of PNVCL and PNVCL-SiO_2 was inefficient, these materials were analyzed by SEM to verify the influences of these polymers in the chitosan structure. This chitosan and its PNVCL hybrids present similar appearance aspects being soft and water-insoluble.

The classification for porous polymer hydrogel defines microporous (<2 nm), mesoporous (>2-50 nm) and macroporous (>50 nm)(GANJI; VASHEGHANI-FARAHANI; VASHEGHANI-FARAHANI, 2010). Chitosan hydrogel is a macroporous material that presents an open channel network that can absorb large amounts of water by capillarity forces. This type of material can swell vary fast and usually show poor mechanical properties. On the other size, it is possible to see the change from the chitosan powder (Figure 4.12 (c)), which before the gelling process, present a high packing structure. With the insertion of PNVCL and PNVCL-SiO_2 (Figure 4.12 d-i) is observed a decrease in the pore size and the formation of sheet-like structures. This physical reticulation occurs when ammonia gas neutralizes the protonated glucosamine group, providing a hydrophilic-hydrophobic transition in chitosan. The

higher porous structure observed in chitosan gel (Figure 4.12 b) is characteristic of the direct contact of chitosan with the gas that neutralizes the chitosan solution and forms a porous insoluble gel structure. With the presence of PNVCL and PNVCL-SiO_2, the contact of chitosan with the NH_3 atmosphere is reduced, and as a consequence, a more uniform is produced. PNVCL and PNVCL-SiO_2 act like surfactants capable of modifying the chitosan gel structure, as observed in Figure Figure 4.12 d-i.

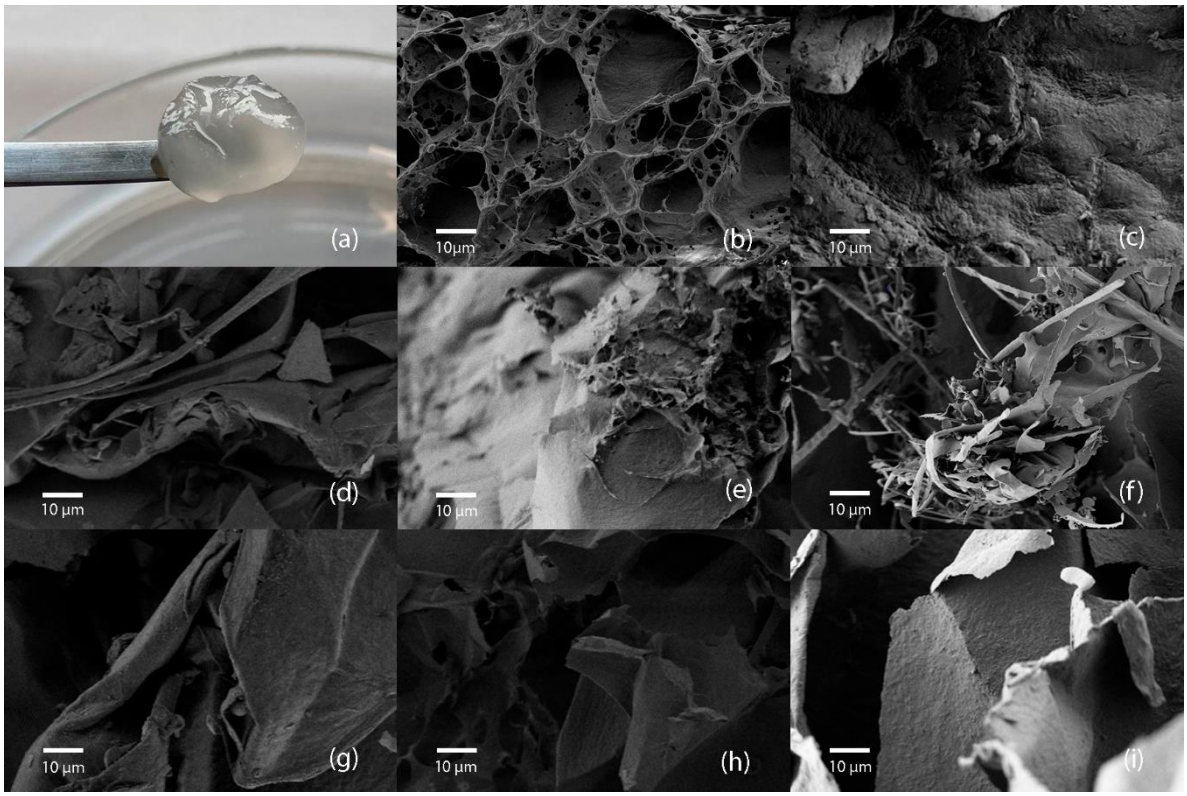

FIGURE 4. 12-Morphological analysis of Chitosan and its hybrid materials.(a) Chitosan gel photograph, (b) freeze-dried chitosan gel, (c) chitosan powder before solubilization, (d) chitosan-PNVCL 3:1, (e) chitosan-PNVCL 1:1, (f) chitosan-PNVCL 1:3, (g) chitosan-PNVCL-SiO_2 3:1, (h) chitosan-PNVCL-SiO_2 1:1, (i) chitosan-PNVCL-SiO_2 1:3.

The development of a DDS for the vaginal application requires some challenges related to the specificities of the vaginal mucosa, the form and texture of the vehicle, and the acceptance by woman public. Concerning this application, a gel should have a good equilibrium between spread in the mucosa and retention in the vaginal channel (T. Yu et al., 2011). Gels structures are largely applied to this purpose because they form a polymer network that can absorb a high quantity of fluid and present viscoelastic properties, which means that it can behave like a solid and a liquid. Because of this, the rheological tests of these gels were studied under conditions like the physiological environment.

According to the synthetic method, chitosan and its composites are completely solubilized in an acetic acid solution before the gelatinization. The viscosity of these solutions was evaluated with the variation of the concentration. According to Figure 4.13, the increase in the concentration of PNVCL leads to an increase in the viscosity of the solutions.

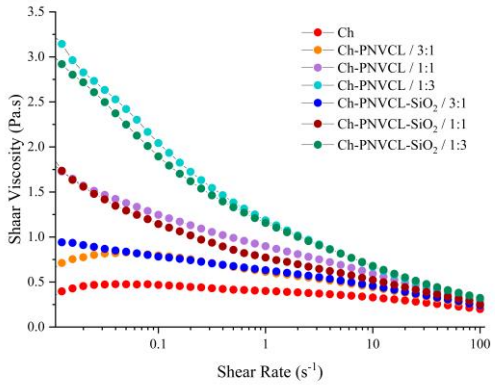

FIGURE 4. 13-Viscosity assay of chitosan and its hybrid materials solution

The oscillatory analysis evaluates the influence of a minor constant strain of frequency, f, over the stress response of a sample. This data is essential to understand the relationship between viscoelastic characteristics with little stress. These tests are typically performed under minor stress because, under these conditions, the relationship between stress and strain is linear. The three-dimensional structure of the gel is not affected under linear viscoelastic region (LVR). The point where the linear relationship between strain and stress stops to be linear is the critical oscillatory stress (τ) indicates a modification of the material structure.

From Figure 4.14 (a and c), it is possible to observe that all chitosan-based materials maintained a linear response of strain with the increase of the stress and consequently presented elevated values of τ around 350 Pa, which means that the gels present high resistant 3D microstructure. All the materials presented lower values of loss modulus (G'') compared to the storage modulus (G'), which is a characteristic of a solid-like structure. The ratio of loss modulus over storage modulus is the tan δ that gives information about the viscoelasticity of the material. Values of tan δ<1 represent elastic gel materials. In Figure 4.14 (b and d), it is possible to see that all materials presented tan δ<<1, which characterizes the samples predominantly like solid elastic behavior over the viscous liquid one because G''<<G'. The advantage

of it in the perspective of a vaginal application is that the polymer structure will not be easily destructed by *in vivo* stress, and the materials can be retained in the vaginal channel for more time, providing the prolonged release of drugs in this site.

On the other hand, these kinds of systems can present limitations during the application because of the poor liquid viscous property on which the vaginal applicators are based. The introduction of this material can lead to the destruction of the 3D structure during the application step, and possibly the gel could not reach the internal genitalia.

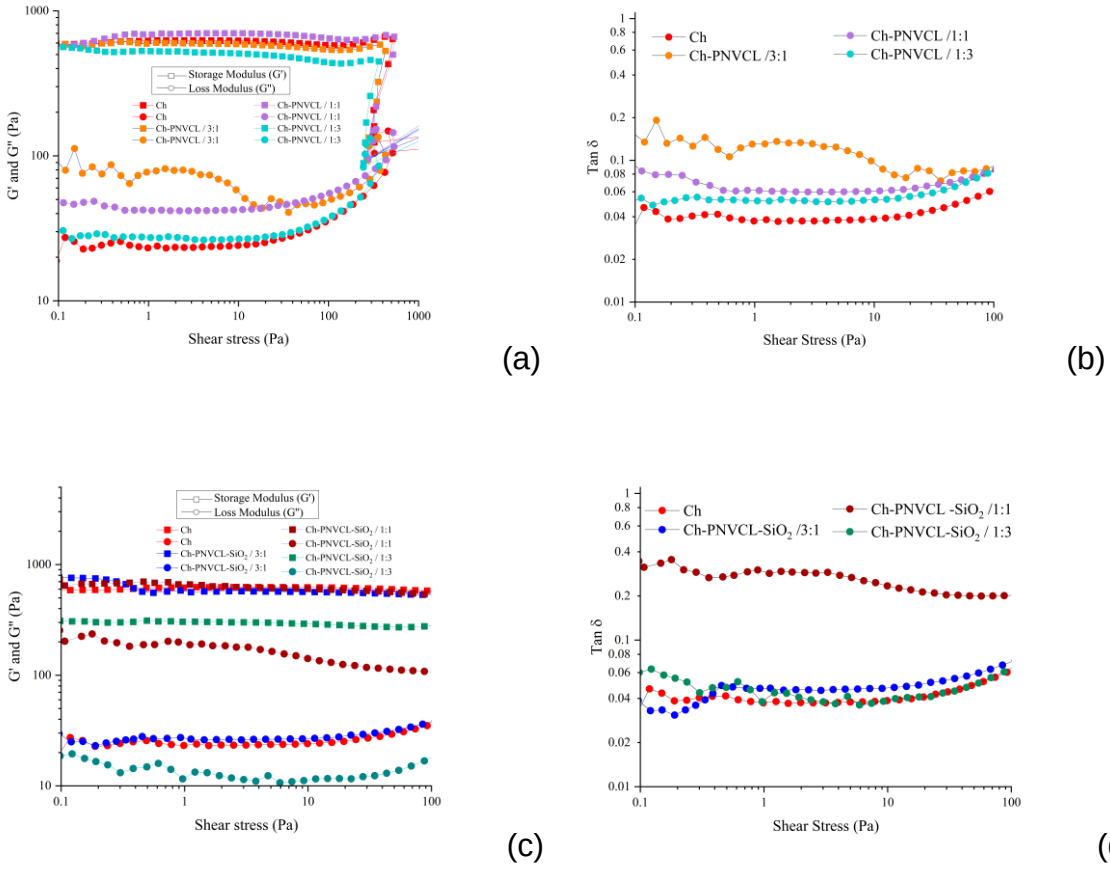

FIGURE 4. 14-Oscillation analysis. G' and G'' vs Shear stress (a) and tan δ vs Shear stress (b) of chitosan and its composites of PNVCL. G' and G'' vs Shear stress (c) and tan δ vs Shear stress (d) of chitosan and its composites of PNVCL-SiO_2.

Considering the chemical and rheological properties of chitosan and chitosan with different concentrations of PNVCL and PNVCL-SiO_2, the association of these polymers have some limitation for a DDS mainly because related to the administration of these gels in the vaginal mucosa. Although, the chitosan physically

crosslinked gel can be dried to form porous sponges. For this reason, this material's physical-chemical and biological properties were also explored.

Two synthesis method was used to synthesize the sponges: the freeze-drying of physically crosslinked gels (CL-Ch) and the solution freeze-drying (UCL-Ch) (HAN *et al.*, 2014a). Both sponges were obtained from the sponge's solution previously described in Table 3.1, and the viscosity was illustrated in Figure 4.13. The FTIR spectrum of sponges obtained by the solution freeze-drying is present in Figure 4.15. Differently from the gels (Figure 4.11), the physical association of chitosan and PNVCL and PNVCL-SiO_2 was efficient. The increase of the bands C=O at 1610 cm^{-1}, N-C stretch at 1480 $cm^{-1,}$ and N-$(CH_2)_2$ stretch at1200 cm^{-1} with the rise of the concentration of PNVCL at chitosan blends indicates the presence that polymer in chitosan structure.

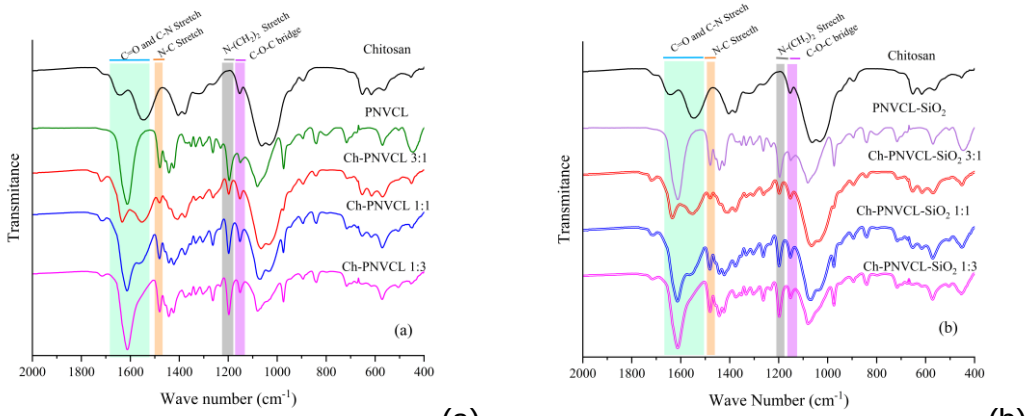

(a) (b)

FIGURE 4. 15-FTIR of chitosan-PNVCL (a) and chitosan-PNVCL-SiO_2 (b) hybrid materials obtained by solution freeze-drying

According to Figure 4.16, the physical association of chitosan sponges and clotrimazole was effective. The vibrational bending of C-H of CTZ aromatic group, C-N stretch, C=C, and C=N stretch were detected in 770, 1081, 1590, and 1560 cm^{-1} for both Ch-CTZ sponges. The same vibrational signs were observed for the composites Ch-PNVCL (Figure 4.15). This is also an indicator of the molecule's stability after the ammonia contact and washing process.

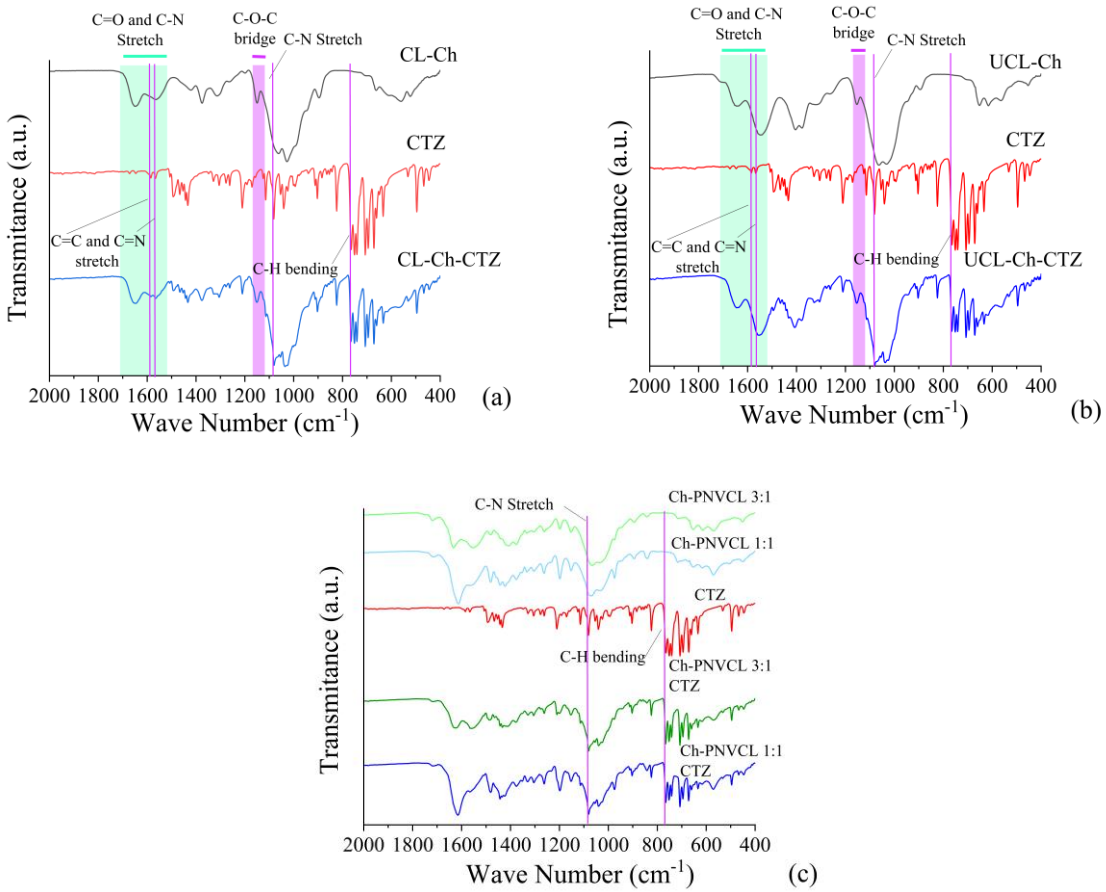

FIGURE 4. 16-Chitosan-clotrimazole sponges synthesized by the physically crosslinked (a),Uncrosslinked chitosan (b) and its composites of PNVCL.

The studies concerning the biomechanical characteristics of the sponges were performed to evaluate the stiffness of the materials from the perspective of a vaginal application. The human vagina is a tubular organ that is subject to different mechanical changes over the women's life. Considering the development of a DDS for the vaginal mucosa, the comfort of the administration is essential, considering the women's acceptability. Considering the type of disease, the direct vaginal route can present advantages considering the therapeutic perspective, for example, avoiding gastrointestinal interactions that can cause the degradation of molecules (PALMEIRA-DE-OLIVEIRA *et al.*, 2022). So, the comfort of the materials was studied considering their compressive stress vs. strain.

Firstly, the compressive test compared the two methods of the obtention of chitosan sponges. The chitosan obtained by the gel and solution freeze-drying presents a stress-strain profile of soft materials in which small compressive stress cause the strain (Figure 4.17). The inserted bar graph shows the Young Modulus (YM)

for these materials at linear elastic region (around 10-30 % of strain), in which no significant (ns) difference was founded. This region is classified as a comfort zone. From the perspective of material for the vaginal application, the materials were considered soft sponges because studies performed with human and animal models show that the vagina is a hyperelastic organ that can support stress in the order of ~10 MPa at comfort zone (around 10-20 % of strain) (RUBOD *et al.*, 2008; RYNKEVIC *et al.*, 2017).

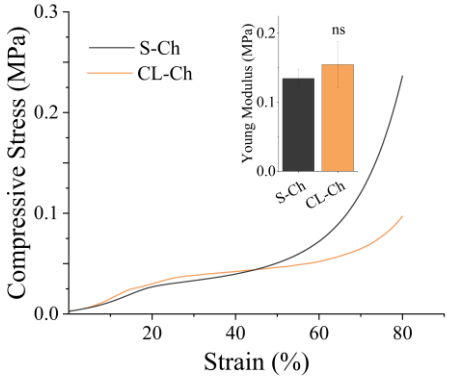

FIGURE 4. 17-Compressive test of Chitosan sponges obtained by freeze-drying polymeric solution (UCL-Ch) and crosslinked gel (CL-Ch).

Considering the Ch-CTZ (Solution and crosslinking), it was observed no significant difference between loaded and empty sponges, although the polymer and the drug have almost 1:1 (W/W) (. This behavior suggests that clotrimazole can act as a lubricant agent because CTZ is a small organic molecule compared to chitosan, and it does not have enough size to participate significantly in the polymeric entanglements.

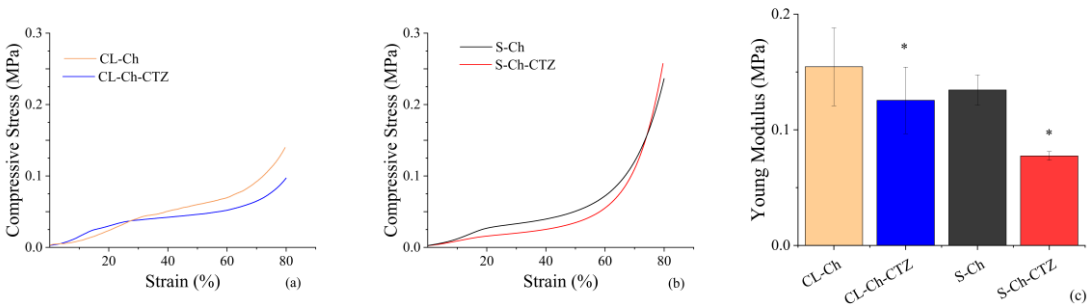

FIGURE 4. 18-Biomechanical properties of Chitosan empty and loaded Sponges. Compressive. test of CL-Ch and CL-Ch-CTZ (a) and S-Ch and S-Ch-CTZ (b) and Young Modulus of empty and loaded sponges (c). * Moderated evidence against the null hypothesis according to paired t-test

According to the previous results of FTIR (Figure 4.11), it was impossible to synthesize gels or sponges of chitosan and PNVCL and PNVCL-SiO_2 using the crosslinked method with control of the mass ratio of the polymer. So, the sponges' chitosan composites with PNVCL and PNVCL-SiO_2 were obtained only by the solution freeze-drying method. These materials' biomechanical properties were evaluated by studying the compressive stress vs. strain behavior (Figure 4.19). Small stress values were necessary to provide a strain, meaning the materials were very soft.

Considering the application, all the materials were considered soft because the maximum compressive stress did not exceed 0.5 MPa without any plasticizer. However, the materials Ch-PNVCL 1:3 and Ch-PNVCL-SiO_2 1:3 was very rigid compared to the other. According to a compressive sensorial evaluation of these materials, they are denser and more similar to a tablet than a sponge. The relationship between the stress and the materials' strain was calculated in the linear elastic region around 10 – 30 % of strain (Figure 4.19 -c). The statistical differences of the PNVCL and PNVCL-SiO_2 compared to chitosan were evaluated. According to this analysis, the presence of pure PNVCL did not significantly affect the YM of chitosan, maintaining the softness of chitosan although the addition of another polymer.

Until the mass ratio of 1:1, no reinforcement was caused by adding PNVCL. However, Ch-PNVCL 1:3 and Ch-PNVCL-SiO_2 1:3 presented the highest YM. This behavior is expectable because PNVCL has an elevated glass transition temperature (T_g) which is also a prediction of its mechanical property that present a rigid amorphous structure under room temperature, and its molecular mobility is reduced (See Figure 4.9). The Ch-PNVCL-SiO_2 1:3 presents a small decrease of YM compared to chitosan. Although no significant effect has been observed for PNVCL at the same concentration, a trend to this decrease is also observed. It can be justified by a difference in the molecular weight of both polymers or a poor dispersion of SiO_2 over the polymeric matrix (ZHANG *et al.*, 2020).

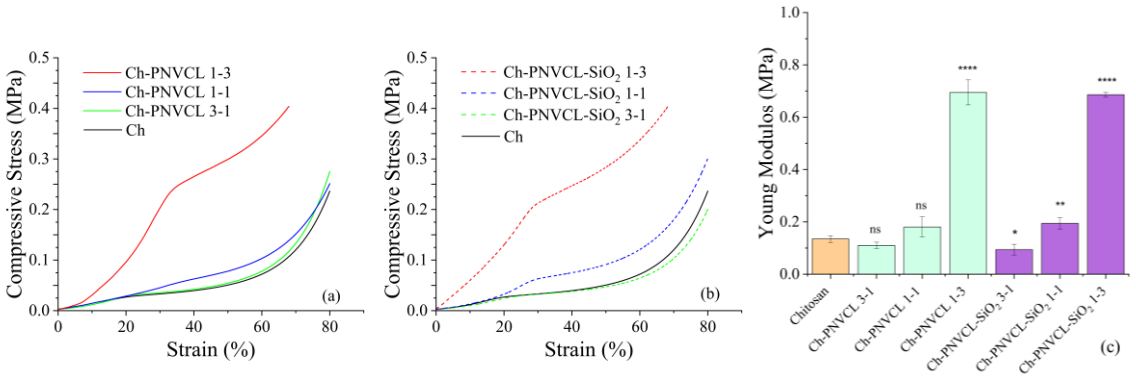

FIGURE 4. 19-Biomechanical properties of Chitosan hybrid Sponges obtained by the freeze-drying of polymeric solution. Compressive test of Chitosan-PNVCL (a) and Ch-PNVCL-SiO_2 sponges (b) and Young Modules of all materials with a different mass ratio of Ch-PNVCL or Ch-PNVCL-SiO_2 (c). * is a p-value range of 0.01-0.05, which indicates moderated evidence against the null hypothesis; ** is a p-value range of 0.001-0.05, which means good evidence against the null hypothesis; **** robust evidence against the null hypothesis

According to the SEM analysis of physically crosslinked and uncrosslinked chitosan, it was possible to observe changes in pore form, size, and distribution. Both chitosan forms scaffold highly porous structures classified as macroporous materials according to the International Union of Pure Applied Chemistry's classification. CL-Chitosan present pores with straight contour and higher pore size compared to uncrosslinked one. The PdI indicates a formation of more regular pore size distribution in CL-Ch. The superior pore size is attributed to the insertion of NH_3 gas in the chitosan during the synthesis process in which the polymer is subject to a sol-gel transition. The ammonia penetrates the chitosan solution modifying not only its cationic behavior but also causes changes in its surface by the gas forming not directly induced(Jahani et al., 2020).

With the addition of clotrimazole, it was observed a thin increase in the PdI of uncrosslinked chitosan (Figure 4.20 h). For the crosslinked one, the growth was much higher, from 0.08 to 0.94 (Figure 4.20 f). This behavior can be justified by the strong chemical interaction of chitosan and clotrimazole obtained by the crosslinking method. The value of association efficiency of 102±8.87 reinforces it because although the several washes, the drug is maintained in a chitosan scaffold. This strong interaction can justify the formation of a compact structure on the surface of the chitosan sponge. The porosity of crosslinked and uncrosslinked chitosan calculated by the displacement method gives a value of 42.08 ± 1.54 and 56.9 ± 6.0, respectively,

which corroborates with the SEM analysis of this highly porous material with a density of 0.029 g/mL and 0.0699 g/mL.

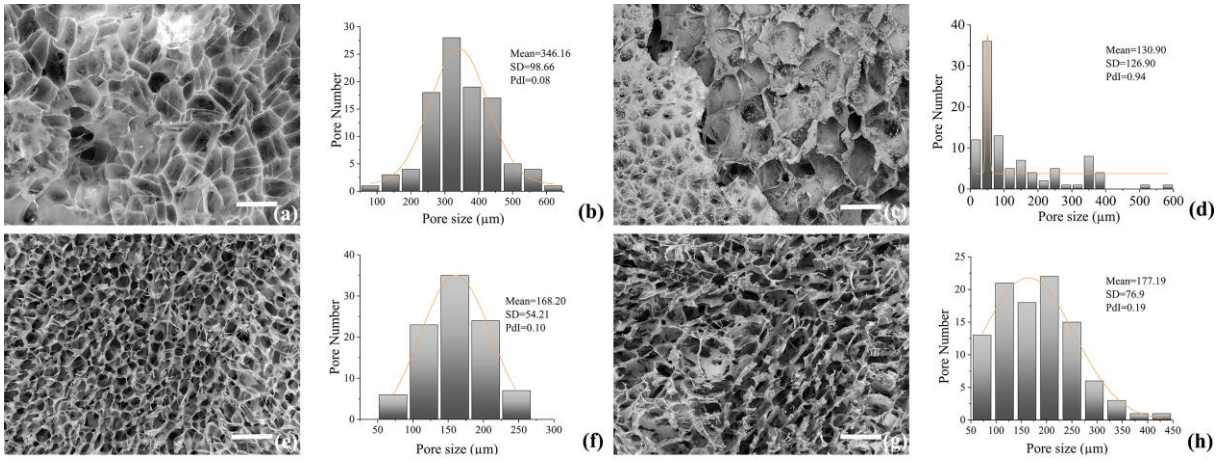

FIGURE 4. 20-SEM analysis of Chitosan sponges. Chitosan sponges synthesized by the physical crosslinking method (a) and its pore size distribution (b). Crosslinked chitosan-clotrimazole sponges synthesized by the physical crosslinking method (c) and their pore size distribution (d). Uncrosslinked chitosan sponges (e) and its pore size distribution (f). Uncrosslinked chitosan-clotrimazole sponges (g) and their pore size distribution (h)

The pore size average of UCL-Ch does not change with the addition of PNVCL, but its polydispersity index increased with the concentration, forming a structure with a heterogeneous pore size distribution (Figure 4.21). A small decrease of pore average is observed in the Ch-PNVCL composites with the addition of CTZ.

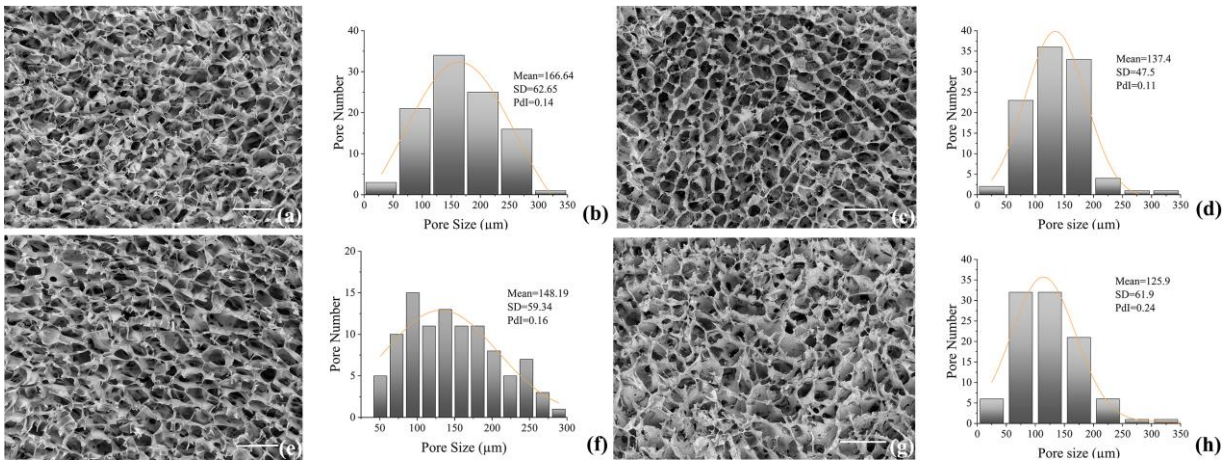

FIGURE 4. 21- SEM analysis of UCL-Ch composites with PNVCL. Ch-PNVCL 3:1 (a) and its pore size distribution (b). Ch-PNVCL 3:1 with CTZ (c) and their pore size distribution (d). Ch-PNVCL 1:1 (e) and its pore size distribution (f). Ch-PNVCL 1:1 with CTZ (g) and their pore size distribution (h).

Table 4.3 summarizes the pore diameter and PdI of all materials and its conjugation with CTZ. It was observed a significant decrease in pore size with the increase of quantity of PNVCL in the Ch-PNVCL composites. This trend is clearly observed in the Ch-PNVCL 1:3 in which the concentration of PNVCL is 3x the concentration of chitosan. In this composite the pore size is 77.83 µm ±22.46. It is also observed that the PdI decreases to 0.08, which means that a more regular and compacted structure is obtained as high as the mass ratio. The same behavior was observed for the composites with PNVCL-SiO_2. The SEM of empty materials Ch-PNVCL 1:3, Ch-PNVCL-SiO_2 3:1, Ch-PNVCL-SiO_2 1:1 and Ch-PNVCL-SiO_2 3:1 is present in the appendix B. All the materials are macropore structured according to the IUPAC classification.

Material	Mean (µm)	PdI
CL-Ch	346.16 ±98.66	0.08
CL-Ch CTZ	130.9 ±126.9	0.94
UCL-Ch	168.2 ±54.21	0.1
UCL-Ch CTZ	177.19 ±76.9	0.19
Ch-PNVCL 3:1	166.64 ±62.65	0.14
Ch-PNVCL 3:1 CTZ	137.4 ±47.5	0.11
Ch-PNVCL 1:1	148.19 ±59.34	0.16
Ch-PNVCL 1:1 CTZ	125.9 ±61.9	0.24
Ch-PNVCL 1:3	77.83 ±22.46	0.08
Ch-PNVCL-SiO_2 3:1	200.18 ±74.9	0.14
Ch-PNVCL-SiO_2 1:1	166.64 ±62.65	0.14
Ch-PNVCL-SiO_2 1:3	92.81 ±23.36	0.06

Table 4. 3 – Morphological properties of the empty and CTZ loaded sponges

4.4 - Biopharmaceutical and biological properties of Sponges

The first step to evaluate the biopharmaceutical and biological properties of gels and sponges was the loading of CTZ inside the scaffolds. After the synthesis of the gel and sponge, the loading capacity and association efficiency was quantified by UV-Vis spectroscopy (Table 4.4). The loading capacity of CL-Ch-CTZ gel was 1.15 % ± 0.02, and its association efficiency was 113.17 %± 1.0. The %LC is near the concentration value of 1% for the preparation of the chitosan gel that is used commercially. The freeze-dried gel which is mentioned as CL-Ch-CTZ sponge,

presented %LC and %AE of 50.5% ± 4.6, and its association efficiency was 102% ± 8.87. These values suggest that the association of chitosan and the drug was efficient, although the several washes after the gelation step in an ammonia atmosphere. The chemical evaluation using FTIR (Figure 4.17) also corroborates this observation. The values of %LC and %AE were calculated according to the CTZ concentration added to the polymeric solution because neither other process stimulates its degradation or removal from the polymeric structure.

Material	%LC	%AE
CL-Ch-CTZ gel	1.15 % ± 0.02	113.17 ±1.0
CL-Ch-CTZ	50.5% ± 4.6	102% ± 8.87
UCL-Ch-CTZ	46.23	100
Ch-PNVCL 3:1	38.92	100
Ch-PNVCL 1:1	30.06	100

Table 4. 4 – Loading capacity and association efficiency of chitosan scaffolds

The microdilution antifungal assay results using DMSO extracts showed that chitosan sponges and their composites with PNVCL caused a slight increase of MIC and MFC values against *C. albicans* ATCC 90028, *C. tropicalis* ATCC 750, *C. krusei* ATCC 6258, *C. albicans* SC5314, *C. glabrata* ATCC 2001 and *C. albicans* ATCC 64550 when compared to the pure drug (Table 4.5) . Differences were minor (no more than two-fold), and the MICs were lower or equal to 16 µg/mL. According to the results obtained so far, the chitosan sponges and Ch-PNVCLs appear to be good DDS in treating VVC due to their high drug-loading capability and maintenance of the activity of pure CTZ. Results are presented as MIC and MFC values against ATCC strains and vaginal isolates of Candida species in µg.mL $^{-1}$ of CLT (n = 3). The azole resistance profile was classified according to fluconazole resistance (FCZ-R) for each strain, is also shown for reference and defined as susceptible (S; MIC ≤ 8 µg mL $^{-1}$); dose-dependent susceptibility (S-DD; MIC = 16–32 µg mL $^{-1}$); or resistant (R; MIC ≥ 64 µg mL $^{-1}$).

Candida's species	FCZ-R	Pure CTZ	CL-Ch-CTZ	UCL-Ch-CTZ	Ch-PNVCL-CTZ 3:1	Ch-PNVCL-CTZ 1:1

		MIC	MFC	MIC	MFC	MIC	MFC	MIC	MFC	MIC	MFC
Albicans ATCC 90028	S	0.5	8	0.5	16	2	16	2	16	2	16
Krusei ATCC 6218	S	2	4	4	4	4	4	4	4	4	4
Tropicalis ATCC 750	S	8	16	16	32	8	32	8	32	4	32
Albicans SC 5314	S	0.5	32	0.5	32	0.5	>16	0.5	>16	0.5	>16
Glabrata ATCC 2001	S	2	16	8	>16	4	>16	4	16	2-4	16
Albicans ATCC 64550	R	2	256	16	>32	8	>32	4-8	>32	4-8	>32

Table 4. 5 - Microdilution antifungal evaluation using DMSO extracts.

The disc diffusion anti-candida assay is a test that evaluates the diffusion of a drug over a plane surface to evaluate the anticandida susceptibility. The advantage of this test is overcoming the limitation related to the insolubility of the drug in the aqueous medium. Figure 4.22 shows the results of the inhibition zone diameter (ZD) of the sponges and the controls (pure disc, FCZ 25 ug, and CTZ 25 ug). This method also has a correlated classification with MIC for categorizing azole resistance. The FCZ with 25 ug is classified as resistant (R; ZD ≤14), dose-dependent susceptibility (S-DD; ZD 15-18); or as susceptible (S; ZD≥19).

For *C. albicans* ATCC 90028 and *C. albican* CS5314, all the materials were classified as susceptible. *Candida krusei* ATCC 6258 was susceptible to CTZ in the control and in the sponges. In the presence of FCZ, the strain was resistant. The azole groups are known to inhibit the enzyme cytochrome P450 sterol 14 α-demethylase (CYP51) present in many fungi and plants (LEPESHEVA; WATERMAN, 2007). This resistance is already reported for *C. krusei* strains, which is mainly associated with decreasingYPG1 sensibility to azole groups(GUINEA *et al.*, 2006). *Candida albicans* ATCC 64550 was resistant to all the conditions, as also reported by Li et al. (LI *et al.*, 2015).

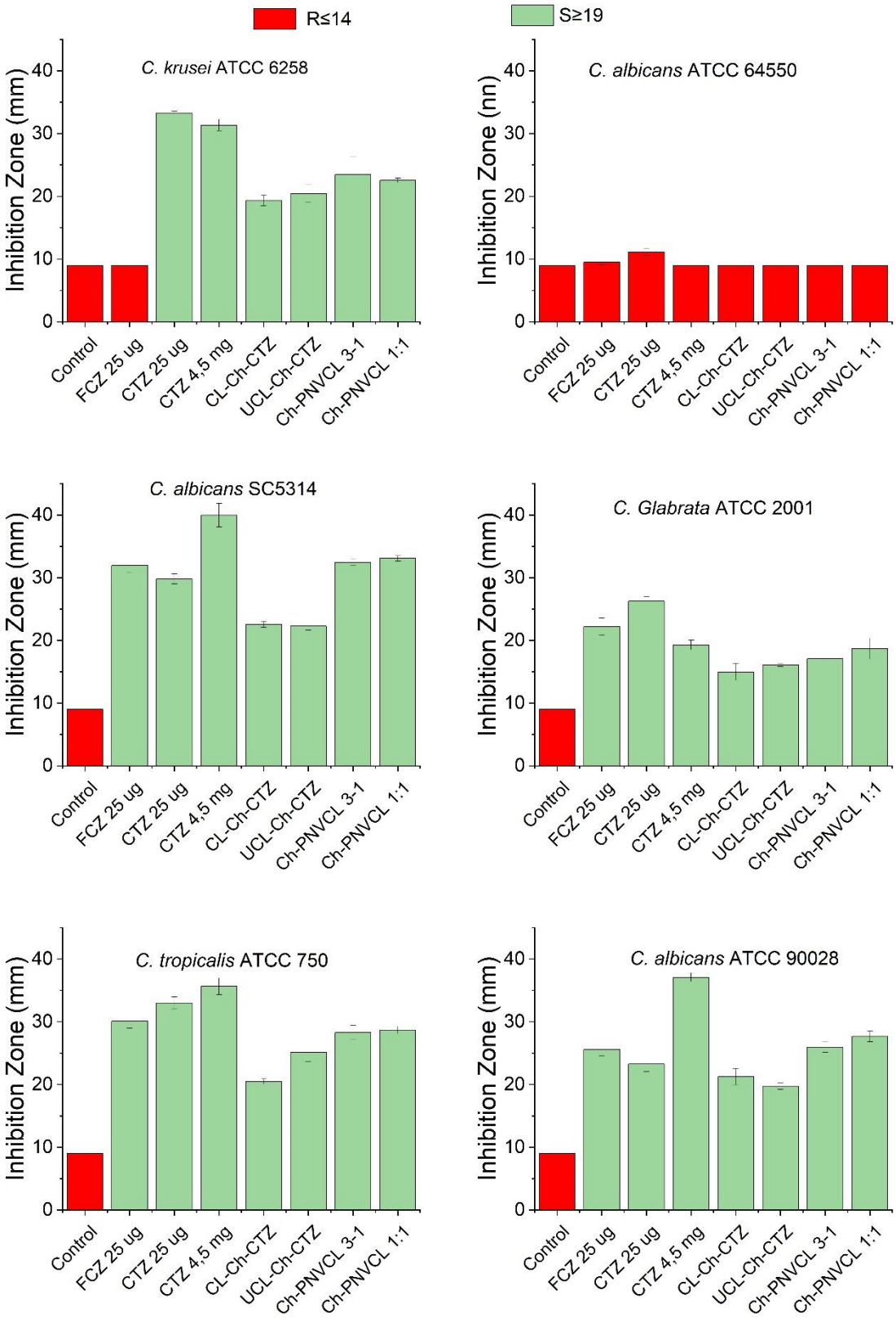

FIGURE 4. 22-Disc diffusion results of standard discs and the chitosan sponges

We also observed that in all experiments, the diffusion zone of chitosan sponges was smaller than in pure disk although they had the same quantity of

clotrimazole (4.5 mg). It suggests that there is a controlled diffusion mechanism associated with the sponges. To understand better this behavior, we performed the water uptake assay under the surface of agar plate. According to this test, the water absorption of the disc was 235.5 % ±3.54 against 586.7 %± 184.3 for CL-Ch-CTZ, 699.3 % ±3.89 for UCL-Ch-CTZ, 1116.8 % ±49.2 for Ch-PNVCL 3:1 and 1055.6 % ± 200.3 for PNVCL 1:1. The moisture uptake of the swelling-polymers participates of the controlled diffusion of the drugs. The solvent penetration through the dried polymer and subsequent drug release can provide a controlled diffusion release of clotrimazole (BRAZEL; PEPPAS, 2000; SOARES; ZUNINO, 2010).

According to the results obtained so far, the chitosan sponges appear to be a good DDS to be used in the treatment of VVC due to their high drug-loading capability and maintenance of the activity of CTZ.

The cell viability of chitosan sponges and their hybrid materials was evaluated using the resazurin method that measures the metabolic activity of living cells. The genital cell lines HEC-1-A and Ca Ski were selected to perform this *in vitro* assay because of their relevance for a vaginal microbicide application. According to the results from Figure 4.23 (a), there is no evidence of cytotoxicity of these materials against both cell lines, which is a prediction of the safety of the scaffolds. Although a trim level of significance appeared for cell viability for some formulations when compared to the control, all the materials were well above the 70% threshold defined by ISO 10993 (INTERNATIONAL ORGANIZATION FOR STANDARDIZATION, 2009). The loaded materials also do not present cytotoxicity *in vitro* against these cell lines, which indicates its potential for application as DDS for vaginal microbicides (Figure 4.23 (b)).

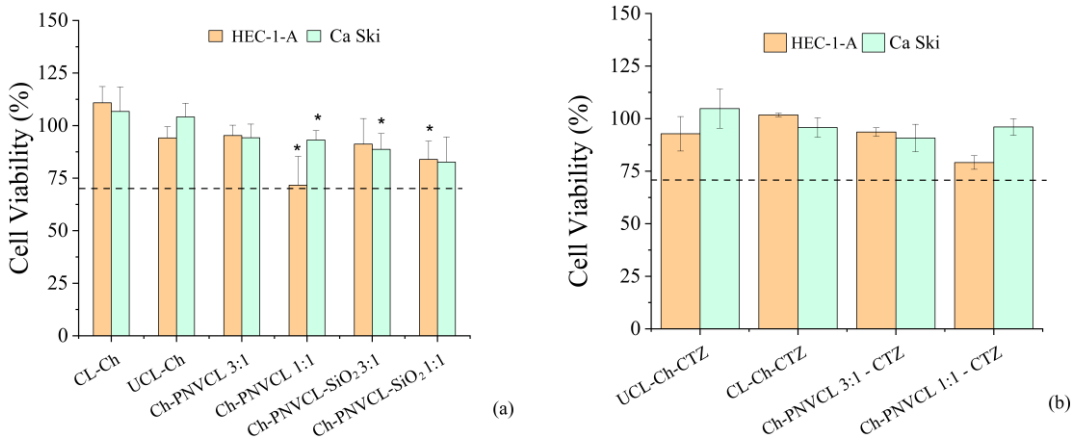

FIGURE 4. 23-Cell viability of empty materials (a) and loaded materials with clotrimazole (b).

The sink conditions were adjusted to allow the dissolution of 3 times the volume of the drug in the scaffold's dosage for the release assay. According to Figure 4.24, CTZ presents a low solubility in pure VFS which gives a saturation volume of 250 mL. Working with 3 x this value (750 mL) could be difficult during the analysis step because the molecule's signal can be impossible to detect. Furthermore, 750 mL is very far to mimic the *in vivo* condition in which about 6 mL of fluid is produced daily (DAS NEVES; AMARAL; BAHIA, 2008b).

To overcome this limitation, the solubility of CTZ was studied with two different surfactants, Poloxamer 407 and Tween 80, to obtain solubility values that can guarantee the sink condition in a saturation volume that represents better the *in vivo* environment. Considering Figure 4.24, VFS with 2% of Tween 80 has the higher solubility, giving a saturation volume of 16,5 mL. With VFS supplemented with 2% of Tween 80, it is possible to perform the drug delivery assay with ~50 mL under sink conditions, which better represents the in vivo environment and is easy to quantify.

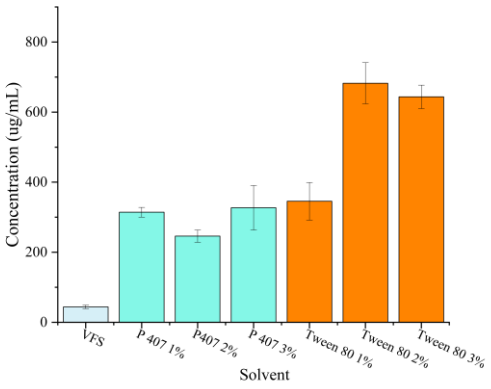

FIGURE 4. 24-Dissolution test using vaginal fluid simulated VFS supplemented with surfactants.

The *in vitro* drug delivery profile was performed for UCL-Ch-CTZ and CL-Ch-CTZ sponges. According to Figure 4.25, the crosslinked sponge presented a fast-release profile. Differently from the UCL-Ch-CTZ, the crosslinked one is not protonated in the glucosamide group because it passes through a neutralization under an ammonia atmosphere. According to the degradation time observed for the CL-Ch-CTZ during the drug release assay (APPENDIX C), the dissolution of this sponge over time was complete at 8 hours because of the scaffold solubilization in an acidic environment. So that is observed that the dissolution mechanism of this material is the self-erosion of the matrix caused by the dissolution of chitosan. A different profile was marked for UCL-Ch-CTZ. With this scaffold it is observed a controlled drug release and the polymer degradation is observed only within 24 hours of the experiment suggesting a diffusion mechanism of delivery (APPENDIX D). When PNVCL is added to UCL-Ch and the Ch-PNVCL 3:1 and Ch-PNVCL 1:1 is used encapsulate CTZ, a similar behaviour is observed with a controlled release of the drug.

To understand better the mechanism of drug release, the mathematical modelling was performed to observe the difference between these for DDS. The drug release profiles of the drug loaded materials were fitted using the kinetic laws zero order, first order, Higuchi, Hixson-Crowell, Ritger-Peppas and Weibull according table.4. 6.

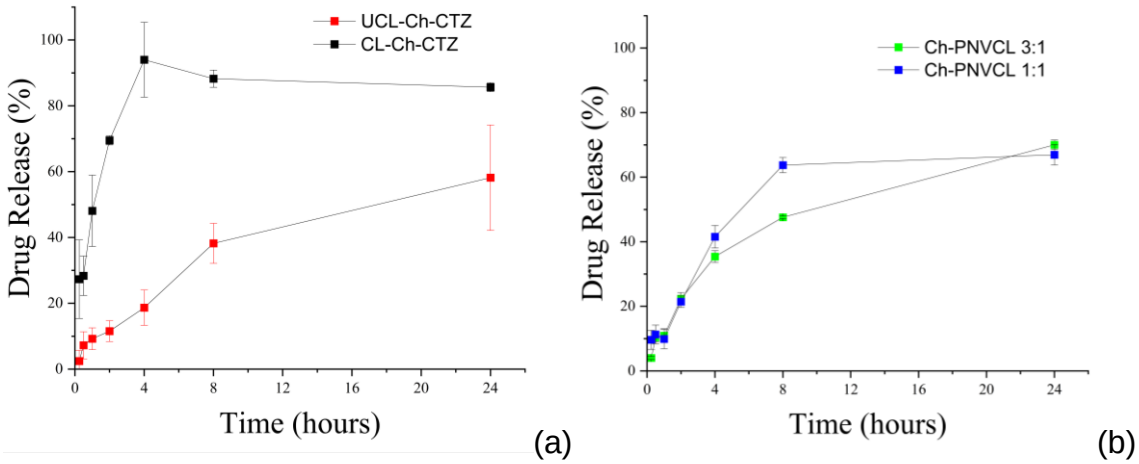

FIGURE 4. 25-Drug release profile of UCL-Ch-CTZ and CL-Ch-CTZ sponges (b) and Ch-PNVCL 3:1 and PNVCL 1:1

Models	Parameters	Materials			
		CL-Ch	NCL-Ch	Ch-PNVCL 3:1	Ch-PNVCL 1:1
Zero Order	R^2	0.280	0.914	0.852	0.681
	K_0	1.532	2.265	2.583	2.454
First Order	R^2	0.316	0.640	0.565	0.574
	K_1	0.015	0.043	0.038	0.033
Higuchi	R^2	0.554	0.977	0.971	0.850
	K_H	13.712	12.925	15.225	15.128
Hixson-Crowell	R^2	0.294	0.947	0.921	0.718
	K_{HC}	0.013	0.010	0.013	0.012
Ritger-Peppas	R^2	0.807	0.959	0.954	0.895
	K_{RP}	0.219	-0.038	0.040	0.081
	n	0.300	0.652	0.614	0.513
Weibull	R^2	0.789	0.967	0.975	0.901

Table 4. 6 – Pharmacokinetics mathematical modelling

CL-Ch was well fitted to Ritger-Peppas and Weibull model with a R^2 equal to 0.807 and 0.789 (Figure 4. 25). The n parameter of Ritger-Peppas was equal to 0.299 that describes a quasi-Fickian diffusion mechanism. The polymer presents a burst release until 4 hours, which is a short interval compared to the entire release process. It means that more administration doses are necessary to achieve a prolonged action against the regrowth of the candida when the concentration is below the MIC. The Ritger-Peppas zero order equation form ($M_i/M_\infty=Kt^n + b$) predict a burst effect b=58.89. This burst release can be desirable only when high FCZ-resistant pathogen is present for example the *C. albicans* ATCC 64550, but for those that are susceptible or dose dependent susceptible, this release rate is excessive. The use of

high drug concentration level can induce resistance and cause cytotoxicity *in vivo.* The better situation is optimizing the drug release according to the MIC value.

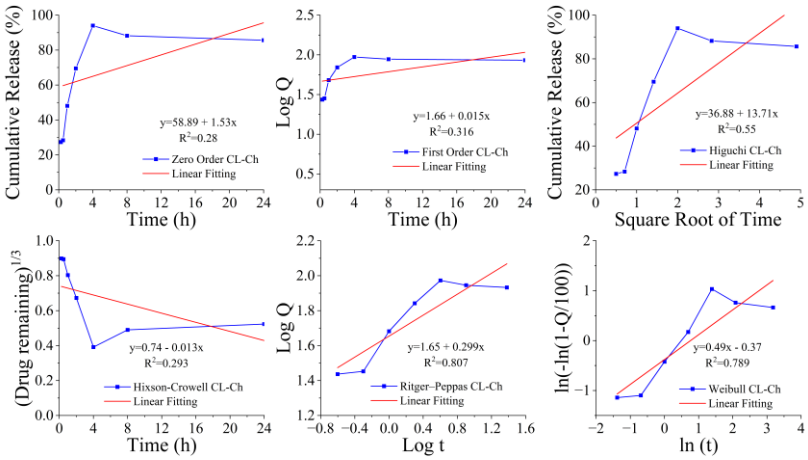

Figure 4. 25 – Mathematical modeling CTZ drug release from CL-Ch sponge

On the other hand, the NCL-Ch was well fitted to Higuchi>Weibull>Ritger-Peppas>Hixson-Crowell>Zero Order (Figure 4. 26). The dissolution process follows a zero-order kinetic profile in which the release rate tends to be constant. The advantage of it is to uniform the drug concentration in the plasma over the release time. The burst factor was 7.93 that is too smaller than the one obtained for CL-Ch, and it means that the release occurs in a more controlled way over the time.

The first order does not describe well this release profile, which means that the drug concentration has no influence under the drug rate. The Higuchi model indicates that the mechanism is governed by diffusion and solubilization from the matrix from a porous structure. The Hixson-Crowell suggest that the dissolution occurs with the erosion of the pharmaceutical surface with the consequent decrease of its volume over the time. This model explains the observed visual decrease of the matrix area over the time for both chitosan sponges.

The Korsmeyer-Peppas n value is also an indicative of which type of mechanism is involved. The n value = 0.65 (n>0.5) describes a non-Fickian anomalous case in which the mechanism governed by diffusion and swelling. It is in accordance with the prediction of Higuchi model concerning the diffusion mechanism.

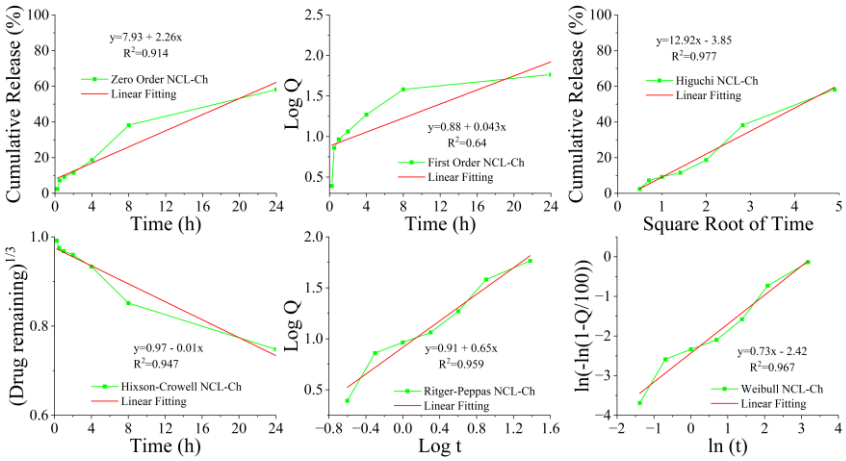

Figure 4. 26 – Mathematical modeling CTZ drug release from UCL-Ch sponge

The drug release profile for Ch-PNVCL 3:1 and Ch-PNVCL 1:1 presented similar behavior compared to NCL-Ch (Figure 4 .27 and Figure 4. 28). Both presented a good fit to Higuchi model that indicates a diffusion mechanism. They presented a little deviation from the zero-order model and a superior β factor, which indicates a faster release compared to the CL-Ch. The Ritger-Peppas n factor for Ch-PNVCL 3:1 and Ch-PNVCL 1:1 was 0.61 and 0.51 respectively, with indicates a diffusion and swelling mechanism. It is observed a trend to the decrease of n factor with the increase of PNVCL concentration from 0.65>0.61>0.51 (NCL-Ch > NCL-Ch-PNVCL 3:1 > NCL-Ch-PNVCL 1:1). The addiction of PNVCL tends to a mechanism governed mainly by diffusion. This can be justified because PNVCL is a water-soluble polymer, and the increase of its concentration decreases the n factor that tends to n=5 (case I) in which the release is governed only by diffusion.

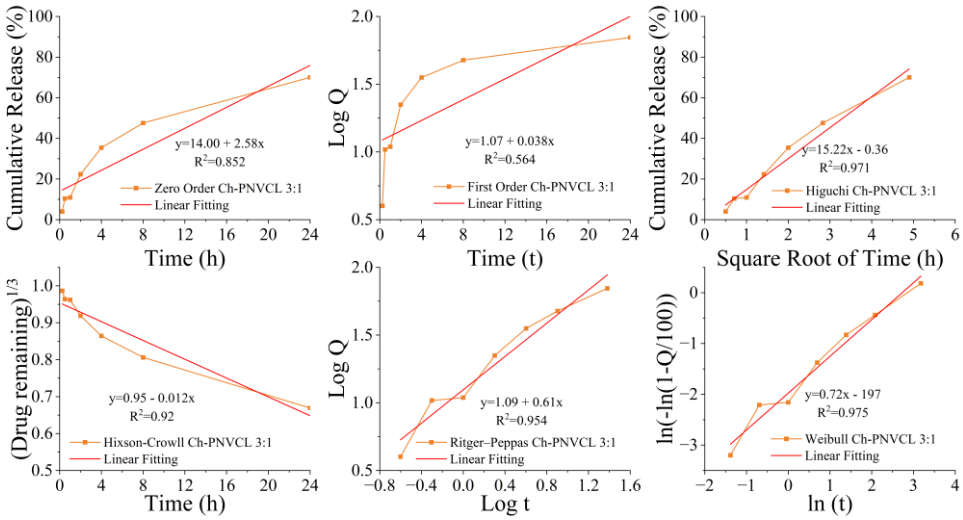

Figure 4. 27 – Mathematical modeling CTZ drug release from Noncrosslinked Ch-PNVCL 3:1 sponge

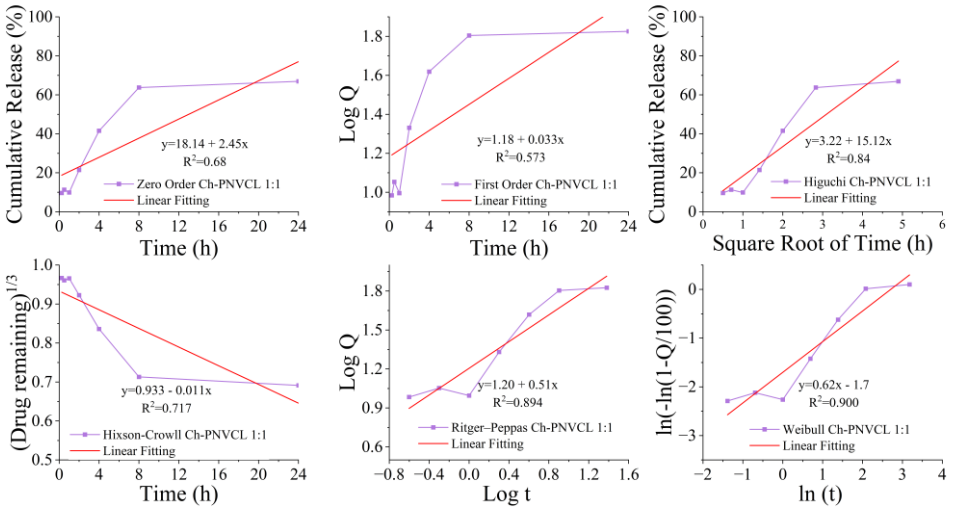

Figure 4. 27 – Mathematical modeling CTZ drug release from Noncrosslinked Ch-PNVCL 1:1 sponge

5 - CONCLUSION

Stimuli-responsive biomaterials based on chitosan, PNVCL, and SiO_2 were synthesized and fully characterized according to their physical-chemical, biomechanical, biological, and pharmacological properties. These studies provide the comprehension and the adjustment of several material properties to the obtention of DDS capable of being applied in the vaginal mucosa.

The biomechanical assay shows minimal differences between the empty and loaded chitosan. The insertion of PNVCL at empty chitosan does not affect its mechanical property until the mass ratio of 1:1. All the materials were considered soft in the application's perspective, which is an important parameter because the comfort of the administration can influence the woman’s acceptability.

All materials are biocompatible with the cell lines HEC-1-A and Ca Ski chosen as models because they are part of the female genital tract. The antifungal activity of clotrimazole is maintained with the polymer association. The drug release in vaginal fluid simulant presents a different profile for the two synthesized chitosan sponges. In one, a fast clotrimazole delivery occurs stimulated by the dissolution of crosslinked chitosan in the medium. The other one presented a controlled drug release.

REFERENCES

ABOUD, Heba M. *et al.* Novel *in situ* gelling vaginal sponges of sildenafil citrate-based cubosomes for uterine targeting. *Drug Delivery*, v. 25, n. 1, p. 1328–1339, 1 jan. 2018. Disponível em: <https://www.tandfonline.com/doi/full/10.1080/10717544.2018.1477858>. Acesso em: 6 dez. 2022.

AK, Gaharwar *et al.* Photocrosslinked nanocomposite hydrogels from PEG and silica nanospheres: structural, mechanical and cell adhesion characteristics. *Materials science & engineering. C, Materials for biological applications*, v. 33, n. 3, p. 1800–1807, 1 abr. 2013. Disponível em: <https://pubmed.ncbi.nlm.nih.gov/23827639/>. Acesso em: 10 ago. 2021.

ALI, Akbar; AHMED, Shakeel. A review on chitosan and its nanocomposites in drug delivery. *International Journal of Biological Macromolecules*, v. 109, p. 273–286, 1 abr. 2018. Acesso em: 10 ago. 2021.

ALMANGOUR, Thamer A. *et al.* Efficacy of clotrimazole for the management of oral candidiasis: A meta-analysis of randomized clinical trials. *Saudi Pharmaceutical Journal*, v. 29, n. 4, p. 315–323, abr. 2021. Disponível em: <https://linkinghub.elsevier.com/retrieve/pii/S1319016421000426>. Acesso em: 5 jul. 2023.

BHATTACHARYYA, Sanjib; WANG, Henson; DUCHEYNE, Paul. Polymer-coated mesoporous silica nanoparticles for the controlled release of macromolecules. *Acta Biomaterialia*, v. 8, n. 9, p. 3429–3435, set. 2012.

BRAZEL, Christopher S.; PEPPAS, Nikolaos A. Modeling of drug release from Swellable polymers. *European Journal of Pharmaceutics and Biopharmaceutics*, v. 49, n. 1, p. 47–58, 3 jan. 2000. Acesso em: 18 abr. 2023.

BRONZE-UHLE, Erika S. *et al.* Physicochemical characterization of albumin immobilized on different TiO2 surfaces for use in implant materials. *Colloids and Surfaces A: Physicochemical and Engineering Aspects*, v. 564, p. 39–50, 5 mar. 2019. Acesso em: 10 ago. 2021.

CAUTELA, Mafalda Pereira *et al.* Composite films for vaginal delivery of tenofovir disoproxil fumarate and emtricitabine. *European Journal of Pharmaceutics and Biopharmaceutics*, v. 138, p. 3–10, 1 maio 2019. Acesso em: 6 dez. 2022.

CAVALHEIRO, Amanda Henriques; COMARELLA, Larissa. *FARMACOCINÉTICA: MODELOS E CONCEITOS-UMA REVISÃO DE LITERATURA PHARMACOKINETICS: MODELS AND CONCEPTS-A LITERATURE REVIEW*. . [S.l: s.n.], [S.d.].

CHEN, Fang; ZHU, Yingchun. Chitosan enclosed mesoporous silica nanoparticles as drug nano-carriers: Sensitive response to the narrow pH range. *Microporous and Mesoporous Materials*, v. 150, n. 1, p. 83–89, 1 mar. 2012. Acesso em: 30 set. 2022.

CORREIA, Maria Almira. Biotransformação de fármacos. *Farmacologia Básica e Clínica - Katzung 12º Edição 2014 HD*. [S.l: s.n.], 2014. p. 53–68.

CORTEZ-LEMUS, Norma A.; LICEA-CLAVERIE, Angel. Poly(N-vinylcaprolactam), a comprehensive review on a thermoresponsive polymer becoming popular. *Progress in Polymer Science*, v. 53, p. 1–51, 1 fev. 2016. Acesso em: 10 ago. 2021.

COSTA, Rayssa H.F. *et al.* α-Cyclodextrin-based poly(pseudo)rotaxane for antifungal drug delivery to the vaginal mucosa. *Carbohydrate Polymers*, v. 302, p. 120420, fev. 2023. Disponível em: <https://linkinghub.elsevier.com/retrieve/pii/S014486172201325X>. Acesso em: 6 dez. 2022.

COSTA, Paulo; MANUEL, Jose; LOBÔ´´, Sousa. *Modeling and comparison of dissolution profiles*. *European Journal of Pharmaceutical Sciences*. [S.l: s.n.], 2001. Disponível em: <www.elsevier.nl/locate/ejps>.

CULVER, Heidi R.; CLEGG, John R.; PEPPAS, Nicholas A. Analyte-Responsive Hydrogels: Intelligent Materials for Biosensing and Drug Delivery. *Accounts of Chemical Research*, v. 50, n. 2, p. 170–178, 21 fev. 2017. Disponível em: <https://pubs.acs.org/doi/abs/10.1021/acs.accounts.6b00533>. Acesso em: 10 ago. 2021.

DAS NEVES, Jos É; AMARAL, Maria Helena; BAHIA, Maria Fernanda. *VAGINAL DRUG DELIVERY*. . [S.l: s.n.], 2008a.

DAS NEVES, Jos É; AMARAL, Maria Helena; BAHIA, Maria Fernanda. *VAGINAL DRUG DELIVERY*. . [S.l: s.n.], 2008b.

DENNING, David W. *et al.* Global burden of recurrent vulvovaginal candidiasis: a systematic review. *The Lancet Infectious Diseases*, v. 18, n. 11, p. e339–e347, 1 nov. 2018. Acesso em: 6 dez. 2022.

DOS, Aniely *et al.* Miconazole-loaded nanoparticles coated with hyaluronic acid to treat vulvovaginal candidiasis. *European Journal of Pharmaceutical Sciences*, v. 188, p. 106508, 2023. Disponível em: <https://doi.org/10.1016/j.ejps.2023.106508>. Acesso em: 5 jul. 2023.

FACCHINATTO, William Marcondes *et al.* Clotrimazole-loaded N-(2-hydroxy)-propyl-3-trimethylammonium, O-palmitoyl chitosan nanoparticles for topical treatment of vulvovaginal candidiasis. *Acta biomaterialia*, v. 125,

p. 312–321, 15 abr. 2021. Disponível em: <https://pubmed.ncbi.nlm.nih.gov/33639312/>. Acesso em: 24 out. 2022.
FERREIRA, Cristina Lorenski *et al.* Biocompatible PCL/PLGA/Polypyrrole Composites for Regenerating Nerves. *Macromolecular Symposia*, v. 383, n. 1, p. 1800028, 1 fev. 2019. Disponível em: <https://onlinelibrary.wiley.com/doi/full/10.1002/masy.201800028>. Acesso em: 10 ago. 2021.
G. KATZNUNG, Bertram. Introdução. *Farmacologia Básica e Clínica* . [S.l: s.n.], 2014. p. 1–13.
GAHARWAR, Akhilesh K. *et al.* Transparent, elastomeric and tough hydrogels from poly(ethylene glycol) and silicate nanoparticles. *Acta Biomaterialia*, v. 7, n. 12, p. 4139–4148, 1 dez. 2011. Acesso em: 10 ago. 2021.
GANJI, Fariba; VASHEGHANI-FARAHANI, Samira; VASHEGHANI-FARAHANI, Ebrahim. *Theoretical Description Of Hydrogel Swelling: A Review*. *Polymer Journal*. [S.l.]: IRANIAN POLYMER JOURNAL (ENGLISH). Disponível em: <https://www.sid.ir/en/Journal/ViewPaper.aspx?ID=171784>. Acesso em: 7 set. 2022. , 1 jan. 2010
GOESMANN, Helmut; FELDMANN, Claus. Nanoparticulate Functional Materials. *Angewandte Chemie International Edition*, v. 49, n. 8, p. 1362–1395, 15 fev. 2010. Disponível em: <https://onlinelibrary.wiley.com/doi/full/10.1002/anie.200903053>. Acesso em: 10 ago. 2021.
GUINEA, J. *et al.* Fluconazole resistance mechanisms in Candida krusei: The contribution of efflux-pumps. *Medical Mycology*, v. 44, n. 6, p. 575–578, 1 set. 2006. Disponível em: <https://academic.oup.com/mmy/article/44/6/575/983420>. Acesso em: 9 abr. 2023.
GUO, Zhengchao; POOT, André A.; GRIJPMA, Dirk W. *Advanced polymer-based composites and structures for biomedical applications*. *European Polymer Journal*. [S.l.]: Elsevier Ltd. , 15 abr. 2021
HAN, Fei *et al.* Preparation, characteristics and assessment of a novel gelatin-chitosan sponge scaffold as skin tissue engineering material. *International Journal of Pharmaceutics*, v. 476, n. 1, p. 124–133, 10 dez. 2014a.
HAN, Fei *et al.* Preparation, characteristics and assessment of a novel gelatin-chitosan sponge scaffold as skin tissue engineering material. *International Journal of Pharmaceutics*, v. 476, n. 1, p. 124–133, 10 dez. 2014b. Acesso em: 13 dez. 2022.
HELMLINGER, Gabriel *et al.* Interstitial pH and pO2 gradients in solid tumors in vivo: High-resolution measurements reveal a lack of correlation. *Nature Medicine 1997 3:2*, v. 3, n. 2, p. 177–182, 1997. Disponível em: <https://www.nature.com/articles/nm0297-177>. Acesso em: 10 ago. 2021.
HOFFMANN, Frank *et al.* Silica-Based Mesoporous Organic–Inorganic Hybrid Materials. *Angewandte Chemie International Edition*, v. 45, n. 20, p. 3216–3251, 12 maio 2006. Disponível em: <https://onlinelibrary.wiley.com/doi/full/10.1002/anie.200503075>. Acesso em: 9 out. 2022.
HOLFORD, Nicholas H. G. Farmacocinética e Farmacodinâmica: dosagem racional e o curso do tempo de ação do fármaco. *Farmacologia Básica e Clínica* . [S.l: s.n.], 2014. p. 37–51.
HUANG, Xiao; BRAZEL, Christopher S. *On the importance and mechanisms of burst release in matrix-controlled drug delivery systems*. *Journal of Controlled Release*. [S.l: s.n.], 2001. Disponível em: <www.elsevier.com/locate/jconrel>.

INTERNATIONAL ORGANIZATION FOR STANDARDIZATION. *ISO 10993-5 - Biological evaluation of medical devices - Part 5: Tests for in vitro cytotoxicity, Geneva, Switzerland.* . [S.l: s.n.], 2009.
INTERNATIONAL ORGANIZATION FOR STANDARDIZATION. *ISO 10993-12 - Biological evaluation of medical devices -Part 12: Sample preparation and reference materials, Geneva, Switzerland.* . [S.l: s.n.], 2012.
INTRA, Jari *et al.* Prevalence and species distribution of microorganisms isolated among non-pregnant women affected by vulvovaginal candidiasis: A retrospective study over a 20 year-period. 2022. Disponível em: <https://doi.org/10.1016/j.mycmed.2022.101278>. Acesso em: 5 jul. 2023.

JAHANI, Babak; WANG, Xinnan; BROOKS, Amanda. Additive Manufacturing Techniques for Fabrication of Bone Scaffolds for Tissue Engineering Applications. *Recent Progress in Materials*, v. 2, n. 3, p. 1–41, 8 set. 2020. Disponível em: <https://www.lidsen.com/journals/rpm/rpm-02-03-021>.
KIM, Hyunjo; FASSIHI, Reza. Application of binary polymer system in drug release rate modulation. 2. Influence of formulation variables and hydrodynamic conditions on release kinetics. *Journal of pharmaceutical sciences*, v. 86, n. 3, p. 323–328, 1997. Disponível em: <https://pubmed.ncbi.nlm.nih.gov/9050800/>. Acesso em: 3 jul. 2023.

KHOSRAVI, A. R. *et al.* Chronic mucocutaneous candidiasis, a case study and literature review. *Journal de Mycologie Médicale*, v. 28, n. 1, p. 206–210, 1 mar. 2018. Acesso em: 29 set. 2022.
LEPESHEVA, Galina I.; WATERMAN, Michael R. Sterol 14α-Demethylase Cytochrome P450 (CYP51), a P450 in all Biological Kingdoms. *Biochimica et biophysica acta*, v. 1770, n. 3, p. 467, mar. 2007. Disponível em: </pmc/articles/PMC2324071/>. Acesso em: 9 abr. 2023.

LI, Xiaofang *et al.* The Rpd3/Hda1 family of histone deacetylases regulates azole resistance in *Candida albicans*. *Journal of Antimicrobial Chemotherapy*, v. 70, n. 7, p. 1993–2003, 1 jul. 2015. Disponível em: <https://academic.oup.com/jac/article/70/7/1993/776696>. Acesso em: 9 abr. 2023.
LIN, Yu-Jung *et al.* Strategies for improving diabetic therapy via alternative administration routes that involve stimuli-responsive insulin-delivering systems. 2018. Disponível em: <https://doi.org/10.1016/j.addr.2018.12.001>.
MAHINROOSTA, Mostafa *et al.* Hydrogels as intelligent materials: A brief review of synthesis, properties and applications. *Materials Today Chemistry*, v. 8, p. 42–55, 1 jun. 2018. Acesso em: 10 ago. 2021.
MEDEIROS, Simone F. *et al.* Solution polymerization of N-vinylcaprolactam in 1,4-dioxane. Kinetic dependence on temperature, monomer, and initiator concentrations. *Journal of Applied Polymer Science*, v. 118, n. 1, p. 229–240, 5 out. 2010. Disponível em: <https://onlinelibrary.wiley.com/doi/full/10.1002/app.32204>. Acesso em: 10 ago. 2021.
MOHAMMED, Marwah N.; BIN YUSOH, Kamal; SHARIFFUDDIN, Jun Haslinda Binti Haji. Poly(N-vinyl caprolactam) thermoresponsive polymer in novel drug delivery systems: A review. *Materials Express*, v. 8, n. 1, p. 21–34, 1 fev. 2018. Acesso em: 10 ago. 2021.
MONTEMBAULT, Alexandra; VITON, Christophe; DOMARD, Alain. Rheometric Study of the Gelation of Chitosan in Aqueous Solution without Cross-Linking Agent. *Biomacromolecules*, v. 6, p. 653–662, 2005.
MORAIS, Renata Pinho *et al.* Skin interaction, permeation, and toxicity of silica nanoparticles: Challenges and recent therapeutic and cosmetic advances. *International Journal of Pharmaceutics*, v. 614, p. 121439, 25 fev. 2022. Acesso em: 18 jun. 2023.
NOROUZI, Mohammad; NAZARI, Bahareh; MILLER, Donald W. Injectable hydrogel-based drug delivery systems for local cancer therapy. *Drug discovery today*, v. 21, n. 11, p. 1835–1849, 1 nov. 2016. Disponível em: <https://pubmed.ncbi.nlm.nih.gov/27423369/>. Acesso em: 6 out. 2022.
PAIS, Pedro *et al.* Membrane Proteome-Wide Response to the Antifungal Drug Clotrimazole in Candida glabrata: Role of the Transcription Factor CgPdr1 and the Drug:H Antiporters CgTpo1_1 and CgTpo1_2* □ S. 2016. Disponível em: <http://www.mcponline.org>. Acesso em: 5 jul. 2023.
PALMEIRA-DE-OLIVEIRA, Rita *et al. Women's preferences and acceptance for different drug delivery routes and products*. *Advanced Drug Delivery Reviews*. [S.l.]: Elsevier B.V. , 1 mar. 2022
PARVEEN, Suphiya; MISRA, Ranjita; SAHOO, Sanjeeb K. Nanoparticles: a boon to drug delivery, therapeutics, diagnostics and imaging. *Nanomedicine: Nanotechnology, Biology and Medicine*, v. 8, n. 2, p. 147–166, 1 fev. 2012. Acesso em: 10 ago. 2021.
PEREIRA, Antonio G.B.; MUNIZ, Edvani C.; HSIEH, You Lo. 1H NMR and 1H–13C HSQC surface characterization of chitosan–chitin sheath-core nanowhiskers. *Carbohydrate Polymers*, v. 123, p. 46–52, 5 jun. 2015. Acesso em: 21 set. 2022.
PILLAI, C. K.S.; PAUL, Willi; SHARMA, Chandra P. Chitin and chitosan polymers: Chemistry, solubility and fiber formation. *Progress in Polymer Science*, v. 34, n. 7, p. 641–678, 1 jul. 2009. Acesso em: 10 ago. 2021.
RAMOS, Jose; IMAZ, Ainara; FORCADA, Jacqueline. Temperature-sensitive nanogels: poly(N-vinylcaprolactam) versus poly(N-isopropylacrylamide). *Polymer Chemistry*, v. 3, n. 4, p. 852–856, 6 mar. 2012. Disponível em: <https://pubs.rsc.org/en/content/articlehtml/2012/py/c2py00485b>. Acesso em: 10 ago. 2021.
REINHOLZ, Jonas; LANDFESTER, Katharina; MAILÄNDER, Volker. The challenges of oral drug delivery via nanocarriers. *https://doi.org/10.1080/10717544.2018.1501119*, v. 25, n. 1, p. 1694–1705, 2018. Disponível em: <https://www.tandfonline.com/doi/abs/10.1080/10717544.2018.1501119>. Acesso em: 10 ago. 2021.
REZAEI, Farnoush Sadat *et al.* Chitosan films and scaffolds for regenerative medicine applications: A review. *Carbohydrate Polymers*, v. 273, p. 118631, 1 dez. 2021. Acesso em: 5 dez. 2022.
RL, Sala *et al.* * Thermosensitive Poly(N-vinylcaprolactam) Injectable Hydrogels for Cartilage Tissue Engineering. *Tissue engineering. Part A*, v. 23, n. 17–18, p. 935–945, 1 set. 2017. Disponível em: <https://pubmed.ncbi.nlm.nih.gov/28384053/>. Acesso em: 29 ago. 2021.
ROBERTS, Jason A.; TACCONE, Fabio Silvio; LIPMAN, Jeffrey. Understanding PK/PD. *Intensive Care Medicine 2015 42:11*, v. 42, n. 11, p. 1797–1800, 3 set. 2015. Disponível em: <https://link.springer.com/article/10.1007/s00134-015-4032-6>. Acesso em: 12 ago. 2021.
ROJZ, Juliana Castilho Chaves *et al.* Photodynamic therapy to control oral candidiasis in a pediatric patient undergoing head and neck radiotherapy. *Photodiagnosis and Photodynamic Therapy*, v. 37, p. 102627, 1 mar. 2022. Acesso em: 29 set. 2022.
RUBOD, Chrystèle *et al.* Biomechanical properties of vaginal tissue: Preliminary results. *International Urogynecology Journal*, v. 19, n. 6, p. 811–816, 2008.
RYNKEVIC, Rita *et al.* Biomechanical and morphological properties of the multiparous ovine vagina and effect of subsequent pregnancy. *Journal of Biomechanics*, v. 57, p. 94–102, 24 maio 2017.
SOARES, João S.; ZUNINO, Paolo. A mixture model for water uptake, degradation, erosion and drug release from polydisperse polymeric networks. *Biomaterials*, v. 31, n. 11, p. 3032–3042, 1 abr. 2010. Acesso em: 18 abr. 2023.

STÖBER, Werner; FINK, Arthur; BOHN, Ernst. Controlled growth of monodisperse silica spheres in the micron size range. *Journal of Colloid and Interface Science*, v. 26, n. 1, p. 62–69, 1 jan. 1968. Acesso em: 10 ago. 2021.
TANG, Fangqiong; LI, Linlin; CHEN, Dong. Mesoporous Silica Nanoparticles: Synthesis, Biocompatibility and Drug Delivery. *Advanced Materials*, v. 24, n. 12, p. 1504–1534, 22 mar. 2012. Disponível em: <https://onlinelibrary.wiley.com/doi/full/10.1002/adma.201104763>. Acesso em: 10 ago. 2021.
TIBBITT, Mark W.; LANGER, Robert. Living Biomaterials. *Accounts of Chemical Research*, v. 50, n. 3, p. 508–513, 21 mar. 2017. Disponível em: <https://pubs.acs.org/doi/abs/10.1021/acs.accounts.6b00499>. Acesso em: 10 ago. 2021.
VIHOLA, Henna *et al.* Cytotoxicity of thermosensitive polymers poly(N-isopropylacrylamide), poly(N-vinylcaprolactam) and amphiphilically modified poly(N-vinylcaprolactam). *Biomaterials*, v. 26, n. 16, p. 3055–3064, 1 jun. 2005. Acesso em: 10 ago. 2021.
WAN, Jiali *et al.* Surface chemistry but not aspect ratio mediates the biological toxicity of gold nanorods in vitro and in vivo. *Scientific Reports 2015 5:1*, v. 5, n. 1, p. 1–16, 22 jun. 2015. Disponível em: <https://www.nature.com/articles/srep11398>. Acesso em: 30 set. 2022.
WANG, Ying *et al.* Mesoporous silica nanoparticles in drug delivery and biomedical applications. *Nanomedicine: Nanotechnology, Biology and Medicine*, v. 11, n. 2, p. 313–327, 1 fev. 2015. Acesso em: 10 ago. 2021.
WU, Juan *et al.* Two cases of primary cutaneous candidiasis caused by Candida parapsilosis: a report and literature review. *Journal de mycologie medicale*, v. 31, n. 3, 1 set. 2021. Disponível em: <https://pubmed.ncbi.nlm.nih.gov/34147759/>. Acesso em: 6 dez. 2022.
WU, Si Han; LIN, Hong Ping. Synthesis of mesoporous silica nanoparticles. *Chemical Society Reviews*, v. 42, n. 9, p. 3862–3875, 15 abr. 2013. Disponível em: <https://www.researchgate.net/publication/235604111_Synthesis_of_Mesoporous_Silica_Nanoparticles>. Acesso em: 30 set. 2022.
WU, Si-Han; MOU, Chung-Yuan; LIN, Hong-Ping. Synthesis of Mesoporous Silica Nanoparticles Chemical Society Reviews Synthesis of mesoporous silica nanoparticles †. *This journal is Cite this: Chem. Soc. Rev*, v. 42, n. 9, p. 3862, 2013. Disponível em: <www.rsc.org/chemsocrev>. Acesso em: 10 ago. 2021.
WU, Juan *et al.* Two cases of primary cutaneous candidiasis caused by Candida parapsilosis: a report and literature review. *Journal de mycologie medicale*, v. 31, n. 3, 1 set. 2021. Disponível em: <https://pubmed.ncbi.nlm.nih.gov/34147759/>. Acesso em: 6 dez. 2022.

YU, Ga er *et al.* Degree of acetylation of chitin and extent of grafting PHB on chitosan determined by solid state 15N NMR. *Macromolecules*, v. 32, n. 2, p. 518–520, 1 jan. 1999. Disponível em: <https://pubs.acs.org/doi/full/10.1021/ma9813338>. Acesso em: 21 set. 2022.
ZHANG, Guigen *et al.* Composites. *Biomaterials Science: An Introduction to Materials in Medicine*, p. 415–429, 1 jan. 2020. Acesso em: 28 mar. 2023.
ZHU, Yicheng *et al.* Design of Thermoresponsive Polymers with Aqueous LCST, UCST, or Both: Modification of a Reactive Poly(2-vinyl-4,4-dimethylazlactone) Scaffold. *Macromolecules*, v. 49, n. 2, p. 672–680, 26 jan. 2016. Disponível em: <https://pubs.acs.org/doi/abs/10.1021/acs.macromol.5b02056>. Acesso em: 10 ago. 2021.

APPENDIX

Medium	Concentration range µg	Equation	R^2
CTZ in DMSO	100-1000	y = 1.4099x + 0.0694	0.9904
VFS	2.4-30	y = 0.0067x - 0.0036	0.9981
VFS P 407 1%	50-250	y = 0.0003x + 0.0072	0.9977
VFS P 407 2%	50-250	y = 0.0067x - 0.0036	0.9909
VFS P 407 3%	50-250	y = 0.0004x + 0.0048	0.9901
VFS Tween 80 1%	50-250	y = 0.0006x + 0.018	0.9929
VFS Tween 80 2%	50-250	y = 0.0006x + 0.0056	0.9995
VFS Tween 80 3%	50-250	y = 0.0011x + 0.0025	0.9961

Appendix A. Clotrimazole calibration curve in different medium obtained by UV spectroscopy.

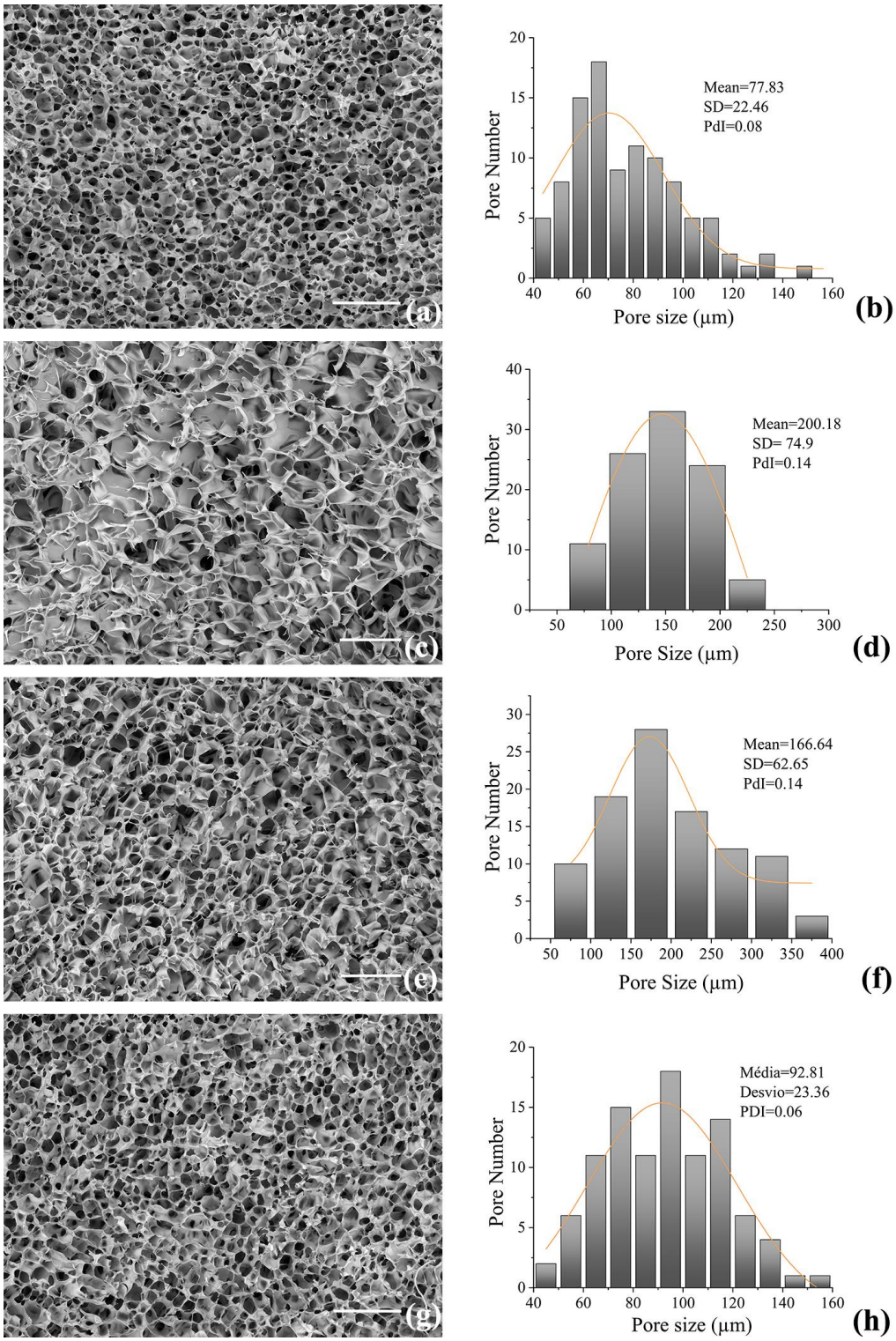

Appendix B. SEM analysis of UCL-Ch composites with PNVCL and PNVCL-SiO_2. Ch-PNVCL 1:3 (a) and its pore size distribution (b). Ch-PNVCL-SiO_2 3:1 (c) and their pore size distribution (d). Ch-PNVCL –SiO_2 1:1 (e) and its pore size distribution (f). Ch-PNVCL 1:3 (g) and their pore size distribution (h).

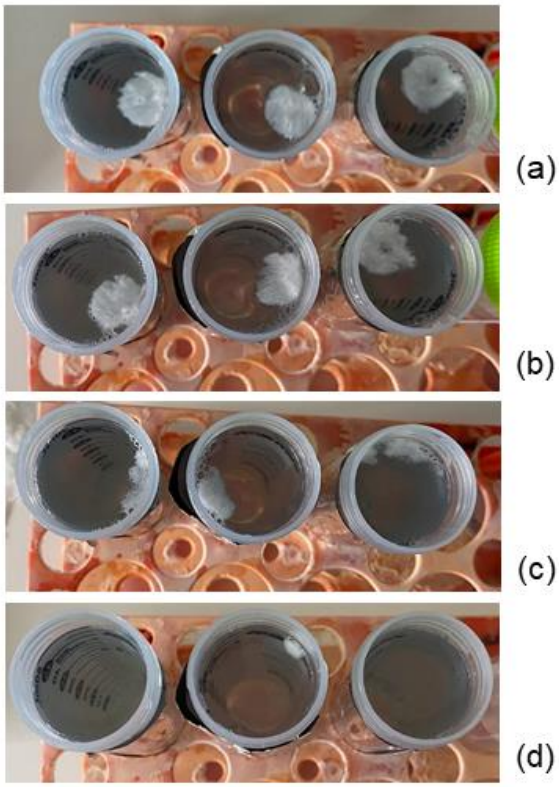

Appendix C. Degradation time of CL-Ch-CTZ during the drug release assay. 30 minutes (a), 1 hour (b), 2 hours (c) and 4 hours (d)

Appendix D. Degradation time of UCL-Ch-CTZ during the drug release assay after 24 hours